Widefield Imaging at Bayfordbury Observatory

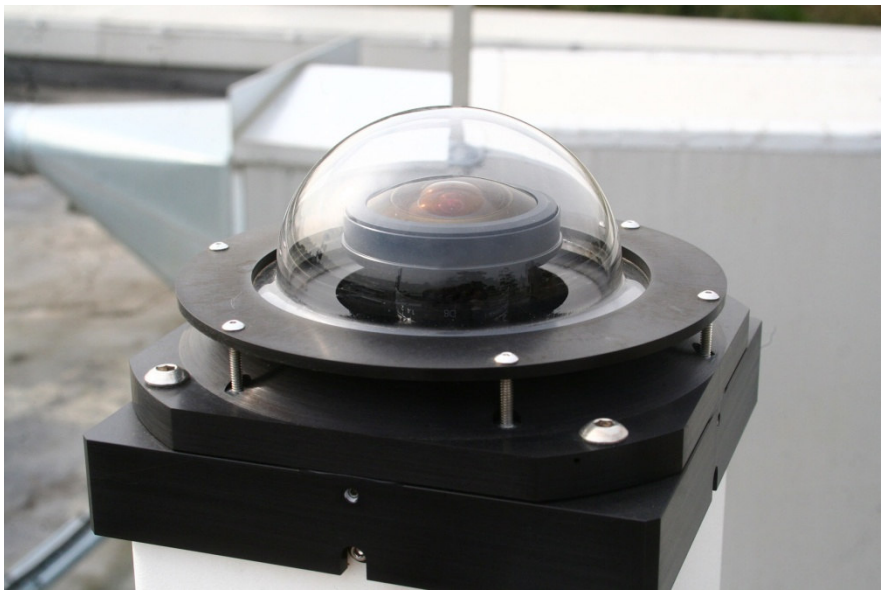

David Campbell

29th April 2010

Supervisor: Professor Hugh R.A. Jones
University of Hertfordshire

Acknowledgments

I would like to thank Professor Hugh Jones for supervising my project, and for his encouragement and guidance throughout.

I also thank Bob Forrest for his help in getting the camera installed and set up, and for checking up on the computer whilst at Bayfordbury, and Becky Wainwright for setting up the web server, and technical support with networking the computers.

I also express my gratitude to the East of England Science Learning Centre for hosting the camera and computer, and to the UH Charitable Trust for funding the camera.

Summary

The all-sky camera is a valuable tool for astronomical observatories, giving an instant picture of the conditions across the entire sky in one clear view.

The University of Hertfordshire's new all-sky camera was set up at Bayfordbury Observatory to enable continual nightly imaging and archiving of raw data, as well as the integration of the near-live images to the internet so that anyone can view the current conditions at Bayfordbury.

The SBIG AllSky-340 camera used gives excellent quality images with very little noise during the typical 30 second exposure time, with no need for active cooling. The field of view of the camera encompasses 95% of the sky and stars down to 5th magnitude can be seen at the Zenith in the unprocessed images, with stars down to 8th magnitude able to be detected using processed raw images.

The camera was set up and run for a period of 6 months from November 2009 to May 2010. During this time the images from the camera were analysed each day to log hourly weather conditions and check for astronomical transient events in the sky such as meteors, supernovae and gamma-ray bursts. In total 26 suspected meteors above magnitude -2 were picked up. Trails and flares caused by satellites were also seen, notably 14 predicted Iridium flares up to magnitude -8 as well as trails caused by the International Space Station and Space Shuttle Discovery.

After analysing the hourly fraction of clear sky over the 6 months, 13.6% of those nights were found to be photometric, 35.7% were spectroscopic, whilst 18.8% had no periods of clear sky at all. A common tendency for the conditions to stay the same was seen, as 66% of hours had the same cloud cover fraction as the previous. However across consecutive nights, it was found that 19% had the same average clear sky value as the previous. Estimations of the fraction of clear sky each hour were initially done by eye, and later a program to automatically analyse the images was also developed, giving the possibility of having the system running autonomously to display previous sky conditions on the website without intervention.

A number of Mira type variable stars were identified for detecting during their periods of maximum brightness, where they peak above naked eye visibility. However due to the large brightness gradient of the sky and the low magnitude of most of these stars, only the brightest star Mira was accurately identified and photometric measurements of it taken. Although greatly limited by the number of photometric nights during the maximum period, these measurements fell within the range of values taken by the American Association of Variable Star Observers.

Contents

Initial Plan

Introduction

For my project I will be using the newly acquired all-sky camera located at Bayfordbury Observatory to constantly monitor the night sky over the period of the project. The camera is an SBIG *AllSky-340C, containing a highly sensitive* Kodak 640x480 pixel CCD and a Fujinon 1.4mm f1.4 fisheye lens giving horizon to horizon coverage[1].

Main Objectives

Constant records of the night sky open up many possibilities, however I have two primary aims for my project. First will be the capture of meteors. As each meteor will be on a specific pixel for a fraction of second (unlike stars) only particularly bright meteor will be detectable on the images, but I hope for there to be enough that several meteor showers can be seen and their radiants, zenithal hourly rate (ZHR) and peak be calculated. There are 3 large meteor showers that occur over the course of the project; the Leonids (peak 17th Nov), Geminids (peak 14th Dec) and Quadrantids (peak 3rd Jan)[3]. All of these have estimated ZHRs of over 100, but the Leonids are of particular interest this year as there have been several predictions of a 'half-storm' with 300, 500 or even up to 1500 meteors per hour. Even if the camera is not fully networked and operational by then I will still try to have it recording over the night of the 17th for this.

My second main objective is to use the camera to monitor the observing conditions, such as cloud cover and limiting magnitude. England is usually perceived as a poor choice of a country to do optical astronomy in due to the adverse climate and large amount of light pollution. Figures from the Met Office give the South of England as having typically 1550-1600 hours of sunshine annually[2] (out of a total possible 4380) which indicates cloud cover about 36% of the time. I would like to examine the impact of the clouds in more detail as a small number of fast moving clouds would limit observations in all areas of the sky, however a large amount of stationary clouds would still allow long exposures in a clear part of the sky. Live images of the sky above Bayfordbury will also be uploaded to a webpage which will allow people planning to observe there to view current weather conditions as well as an animation of the previous set of frames to see if conditions are getting better or worse. It can also be a useful aid for people at the observatory to monitor the sky conditions as the camera can pick up clouds below naked eye visibility.

Secondary Objectives

Depending on the limitations of the camera (yet to be explored) I would also like to do some other investigations using the data. Mira type variable stars are a potential good candidate to observe. Their brightness can vary by up to 11 magnitudes over the course of several hundred days. I have identified 7 initial possible candidate stars which should be visible by the camera during their peak brightness and the 6 month period I will be taking data and will hopefully allow me to construct part of their light curves. These are; o Cet, χ Cyg, R Leo, U Ori, R Cas, α Her and R Lyr[4]. These may be added to or removed from subject to the results of the initial investigation into the limitations of the camera. R Leo and U Ori will be visible over the whole 6 months, the others will become too low to observe by January or February.

The constant recording of the night sky would also be ideally suited to monitoring for sudden events in the night sky such as novae, supernovae and comet outbursts as with Comet Holmes in 2007. Whilst these events are rare and being the first to notice one yet rarer, if one were to occur then images of the event unfolding from the start may be few and far between, and sought after. It would also be interesting to try and find another similarly run camera located some distance away from Bayfordbury which could be used to calculate a rough flight path triangulation in the event of a fireball.

Methodology

My initial investigation will be to find the limits of the camera, mainly the lowest magnitude object observable. This will allow me to possibly use the data from the camera for other uses. The camera will be connected to a computer which will be set to take images continually so that at night the only gap in recording will be the 1 second taken for the camera to read the CCD[1]. Continual coverage is essential to capture as many meteors as possible, as well as being able to track the large amounts of planes that fly over Bayfordbury to be discounted. A partial capture of a plane trail due to a gaps in imaging can be mistaken for a meteor trail, however if the slower moving plane is capture in two continual frames it can be easily identified as a plane. The images will then be saved to an FTP account where each day I will download them and save them locally as a backup and so I can analyse them further. I will then make an animation of the previous night's frames to allow me to easily check for bright meteors or other events. Frames at set intervals will be analysed to determine the percentage cloud cover as well as the limiting magnitude. I intend to use SBIG CCDOPS to do astrometry and photometry work on the FITS files for variable star analysis. To create animations and do frame by frame checking for meteors I intend to use Jasc Animation Shop. Due to the very large amount of data I will be collecting over the 6 months it will be much easier to continually analyse the data soon after it is collected. Quick inspection of the images will also be essential if any novae, supernovae, fireballs or similar events ever occur.

Timetable

17th November 2009 – Camera recording at night for the possible Leonid 'half-storm'

30th November 2009 – Camera fully operational and networked, regular archiving begins

10th December 2009 – Poster presentation

17th January 2010 – Completion of the analysis of the Meteor showers data

7th February 2010 – Complete analysing data for the early set of variables stars

26th February 2010 – Sample chapter and contents page

31st March 2010 - Complete analysing data for the late set of variables stars

11th April 2010 – Culmination and final completion of the analysis of observing conditions

29th April 2010 – Project report handed in

May 2010 – Project viva

Introduction

The University of Hertfordshire has recently acquired an all-sky camera for use at its astronomical observatory at Bayfordbury. During the course of this project I will set up the camera so it can continually take images throughout each night and archive them to a local computer.

Files will also be also be uploaded to a remote web server to enable remote download of files daily across the internet as well as integrating the images into a website, to allow live monitoring of the current conditions from around the world.

Daily records on the weather conditions will be calculated to enable statistics to characterise the observing site so that it may be compared to others. This may also be able to be automated so that it may continually monitor the sky and generate statistics on weather conditions without the need for human intervention.

A number of bright variable stars will be visible during the period of analysis, and it is a further aim to be able to continually record these to generate light curves as the peak in brightness.

Having an archive of the sky for every night will also allow for monitoring of transient objects; meteors and satellites, as well also watching for celestial changes such as bright gamma-ray bursts and supernovae.

1) Setting up the Camera

Camera details and specifications

The camera used is the third version of the All Sky camera manufactured by the Santa Barbara Instrument Group (SBIG). Called the AllSky-340, the optical system consists of a Kodak KAI-0340 CCD sensor and a Fujinon FE185C046HA-1 lens [1]. The KAI-0340 is a VGA resolution (640x480 active pixels) 1/3" format CCD with 7.4µm size square pixels [2]. The FE185C046HA-1 is a wide angle fish-eye lens with a focal length of 1.4mm and a focal ratio range of f/1.4 to f/16 [3] fixed open at f/1.4 in the AllSky-340 [1]. This combination of fast focal ratio and large pixel size gives it excellent sensitivity. This combination gives a field of view of 185°×144°47' [3] and resolution of 18' per pixel. Assuming the camera is aimed at the zenith, a maximum of 95.0% of the area of the sky can be imaged, with 2.52% cut off at the top and bottom. The areas around the edges are most affected by light pollution and not suitable for any measurements so this loss is not too detrimental.

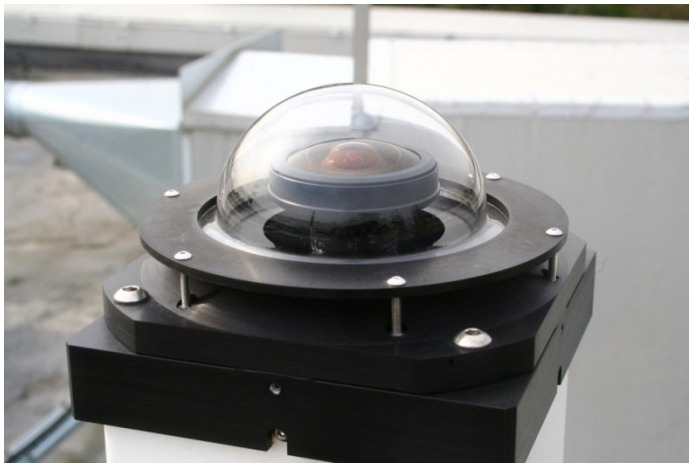

Figure 1: Close-up of the camera showing the fisheye lens, acrylic dome and focusing plate.

The camera is located on the roof of the East of England Science Learning Centre, next to the University of Hertfordshire's astronomical observatory at Bayfordbury, Hertfordshire (51.776N 0.096W). The elevated vantage point from the roof gives it a clear view of the skies, uninterrupted by most of the surrounding trees.

Figure 2: The location of the camera on the roof of the Science Learning Centre, providing a near-interrupted view of the sky.

The camera is connected to a computer inside the Science Learning Centre, via an RS-232 serial cable. Whilst a RS-232 link is slower than USB, it has the advantage of faring better over longer distances, as the cameras are often located far from a computer. Using a USB-serial adapter at the PC end the maximum download speed of 460.8 Kbaud could be achieved. At this rate the average download time of an image is 16.5 seconds.

The lens is protected from the constant effects of the elements (and birds) by a replaceable acrylic dome. The dome is also warmed at night by a heated metal plate surrounding the lens in order to stop dew from forming and to dry off raindrops faster. This heat proved not to be sufficient for the harsh English winter, which also turned out to be the coldest for 31 years [4] and so an additional source of heat was provided via a light bulb positioned in the underside of the camera.

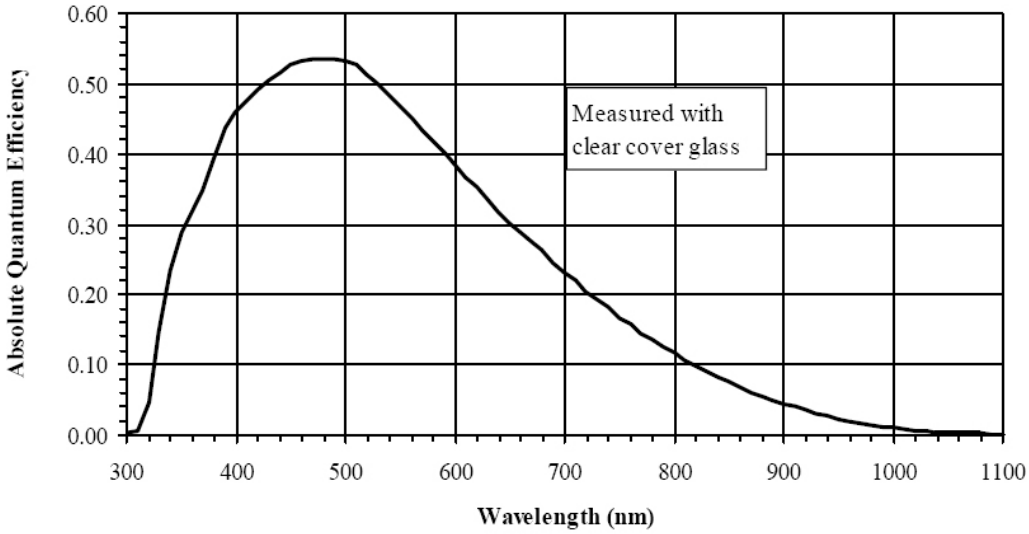

Figure 3: Quantum efficiency curve of the Kodak KAI-0340 [2].

The CCD is unfiltered and so is several times more sensitive than the colour version of the camera which is also available. The spectral sensitivity curve of the CCD seen in Figure 3 shows that response of the camera extends beyond the range of the optical region into the ultraviolet and near-infrared, the ultraviolet however is attenuated by the protective acrylic dome. The extension into the near-infrared allows for dimmer and lower temperature stars to be better detected, without increasing the overall background level, which is largely composed of the light pollution concentrated at the 589nm Sodium doublet lines. The CCD is most sensitive to optical wavelengths, peaking in the blue region at about 475nm.

The limiting magnitude of the sky in the image is largely governed by the light pollution from nearby towns causing a strong gradient from the horizon to the zenith. Although the intensity of the light pollution around the horizon varies, the largest sources correlating with the directions of the nearby towns of Welwyn Garden City, Hoddesdon and Waltham Cross, in all directions the gradient follows a similar intensity curve as shown in Figure 4.

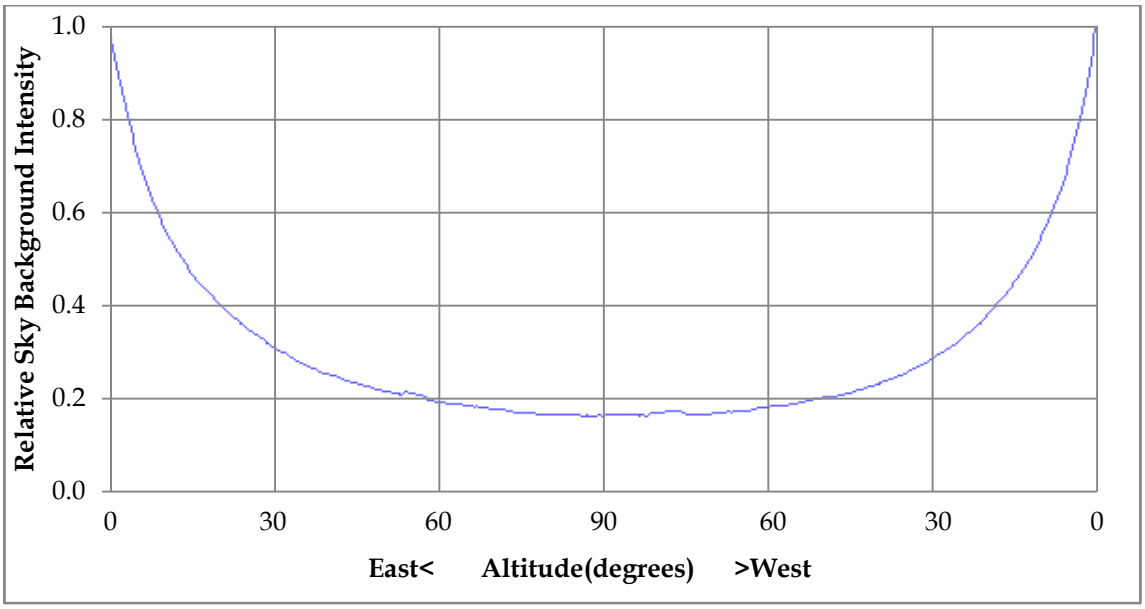

Figure 4: The relative intensity of pixel values (where 0 is no photons detected, and 1 is the brightest part of the sky) of the sky background as a function of altitude above the horizon, measured as a strip from East to West.

This curve follows very closely to the exponential decay function given in Eq.1 where h is the altitude above the horizon in degrees:

$$\boldsymbol{I = 0.838e^{-\frac{h}{5\pi}} + 0.162} \qquad \textit{Eq. 1}$$

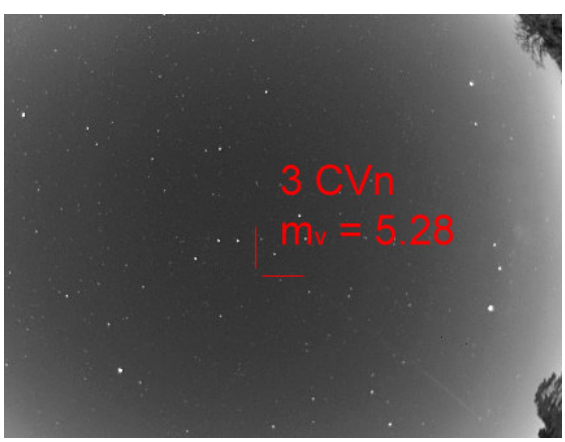

Figure 5: 3 Canum Venaticorum, one of the dimmest stars visible at the zenith in a JPEG image, with no further processing.

In an unprocessed JPEG image taken from the camera, the dimmest stars visible at maximum exposure at the zenith on a clear night is between 5th and 6th apparent visual magnitude – approximately equal to that of the naked eye in good skies.

By stacking 5 uncompressed FITS images and using further processing to remove the background gradient and further stretch the image, stars as low as 7th and 8th apparent visual magnitude could be made out. This is also limited by the noise due to a limited number of cloudless images at a single local sidereal time available to stack. Due to the distortions of the fisheye lens, images at different local sidereal times could not be simply rotated to stack them onto others, and therefore only those taken with a minute of the local sidereal time were suitable.

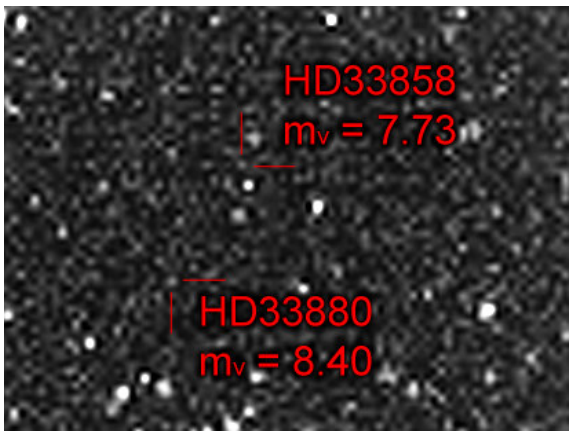

Figure 6: Stars HD33858 and HD33880, examples of the dimmest stars detectable using the FITS images.

Camera and software setup

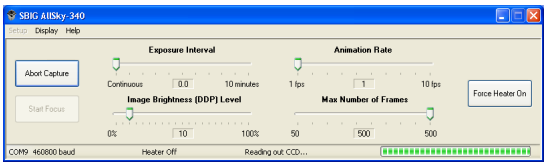

The camera is connected to the operating computer via a RS-232 serial link. To utilise the full download speed available, this is connected to the computer using a USB to serial converter, rather than using the computer's motherboard serial port. If the computer used cannot connect to the camera, it may be that a different USB-serial converter may be needed. The initial CH-340 type one first used only worked on two of the three computers tried, whereas the Prolific PL-2303 used in the end worked well on all three computers.

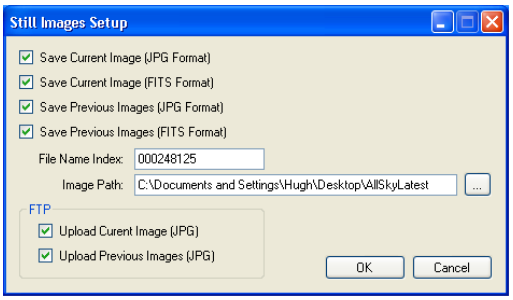

Once connected, the download speed is increased to 460.8Kbaud to allow near-continuous imaging during clear moonless times.

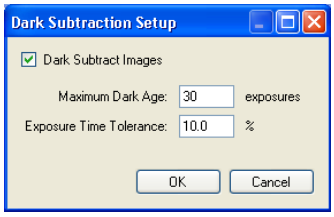

In the still images setup, found in the setup menu, all boxes are checked to enable saving of all previous files, both JPEG and FITS as well as to the FTP server. In the FTP setup the details of the FTP server should be entered, and deletion of files after a certain time be turned. Images should be dark subtracted to remove hot pixels and noise. The settings used were a maximum time between new dark exposures of 30 exposures (~10 minutes) or a change in exposure time of up to 10%. If meteor trail detection is the main use of the camera, the 5Hz chopper shutter can be turned on to differentiate meteor trails for slower ones such as planes and satellites. However, as this shortens the time for which stars are recorded on the chip compared to the recorded time in the FITS header, photometry will no longer be able to be performed. The heat schedule was set from 4pm to 8am, to remove condensation at night. Finally it is important to turn of the Debayer image option in the display menu when using the monochrome version of the camera.

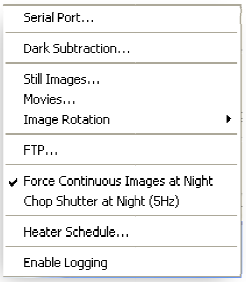

Storage of data and archiving

Important considerations had to be paid to the storage of the images. Left running continuously the camera will take up to 4,500 images each day if the exposure times are not lengthened by periods of clear skies at night. As each JPEG image has an average file size of 58KB and each FITS image has a file size of 605KB, the total size of images downloaded daily to the imaging computer is up to 2.9GB, and around 250MB of JPEG images also uploaded to the web server.

To control the amount of disk space used, a PHP 'housekeeping' program was written to run on the imaging computer and during daytime hours (in order to avoid disrupting the download of important night-time images) scans the directory where the latest images have been downloaded to and deletes all those taken between the hours of sunrise and sunset. Images taken whilst the sun is up are overexposed except during overcast conditions and the short exposures mean than the sky is only exposed for less than 0.003% of the time, and may be deleted to save disk space. In addition the program archives the images into separate directories for each night to aid in organisation. Typically 2,200 images are taken each night, amounting to around 1.4GB of disk space daily or 500GB yearly. Daytime images are also deleted from the web server, however there is a buffer time of 2 weeks to make allocations for the possibility of capturing a rare event during the daytime such as the long-lasting ionisation trail from a fireball/bolide.

JPEG images may also be encoded as an MPEG-4 video for further compression. The resultant video is around 8 times smaller than the total of the JPEG image file sizes, typically 8-12MB. Encoded at 25 frames per second, the videos are around a minute in length and allow for quick and easy viewing of an entire night's worth of images. If disk space becomes a concern in the future, or the continual storage of old images is deemed no necessary then they me simply be stored as a video only. Individual frames may then be extracted if needed, whilst still retaining reasonable detail.

Web integration

To make the data produced from the camera easily accessible to users of the observatory or anyone else interested in current or past conditions at Bayfordbury a small website was created. The home page displays the latest image taken with the camera, which is set to refresh every 20 seconds – around the minimum time it takes to download and process a new image from the camera.

A program was written in PHP to provide an overlay to the live image which displays right ascension and declination coordinate lines, constellation lines and constellation labels. This would aid those unfamiliar with the night sky in gauging the orientation of the images, as well as when clouds obscured major constellations. To overlay the constellation lines, firstly the time the current image was last modified (i.e. the time it was uploaded) was obtained and this converted to the Julian date. Knowing this time and the longitude and latitude of the camera, the altitude and azimuth of the stars joint together by the constellations could be calculated from their right ascension and declinations [5]. These coordinates were then transferred to the 2D plane of the image using the Lambert Azimuthal Equal-Area Projection [6] which was found to provide a good initial fit. These coordinates then had to be rotated and shifted to account for the fact that the camera does not actually point precisely at the zenith, nor is the top well aligned with North. Finally an empirical factor was applied to the coordinates in the x and y direction to compensate for the distortion created by the lens. This was found by plotting stars using the preliminary projection and measuring the error between the plotted stars and their corresponding background star. The errors as a function of the x, and then y directions were fitted to a cubic function and these added to the coordinates. The final result aligns well to the background stars in the central parts of the image, and slightly less well fitting around the edges, however it is still possible to improve the final stretch factor with enough time. In addition the positions of the Moon, Venus, Mars, Jupiter and Saturn were calculated so they could also be plotted onto the overlay.

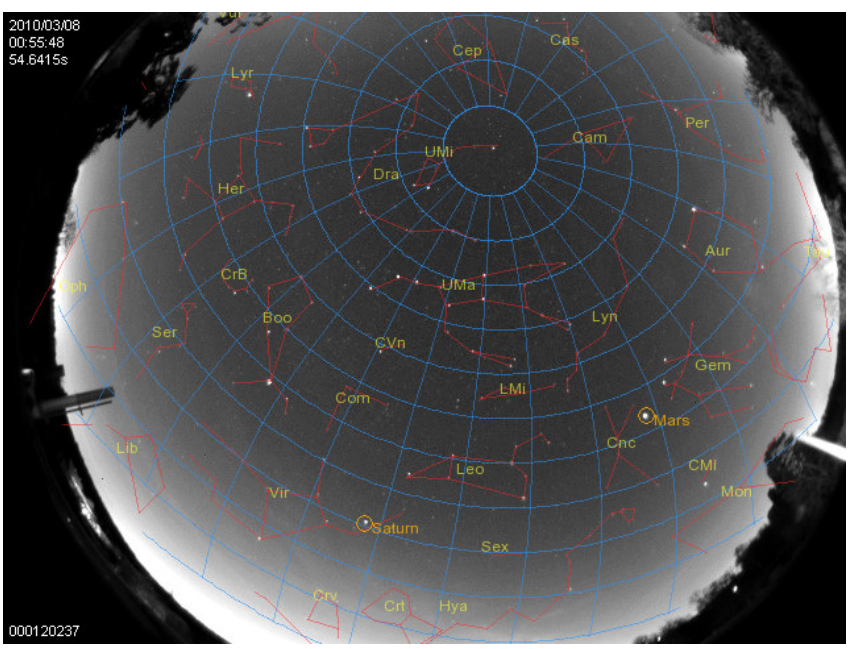

Figure 7: The overlay on an image during a clear night, showing celestial coordinates lines, constellations and two bright visible planets.

Additionally the website contains an archive of viewable time-lapse videos for each night, organised by month. This allows anyone to quickly find out the conditions at Bayfordbury at any time of any night. The MPEG-4 archived videos were reencoded in the Adobe Flash video format to reduce the size by around 2.5 times, and allow wide internet browser compatibility without the need to download and install new video codecs. There is also a page containing interesting images taken with the camera such as meteors, satellites and atmospheric phenomena like lunar coronas.

Figure 8: A screenshot of the home page of the website, with the latest image displayed.

Website link: http://bus-winsrv2.herts.ac.uk/AllSky/AllSky.htm

2) Sky Conditions

Measuring Useful Hours of Clear Sky

Accurate statistics on the amount of time optical observations can be made are an important part of the characterisation of an astronomical observing site such as Bayfordbury. A range of statistics is also necessary as different future developments of the site will have different requirements; for example stellar spectroscopy can be performed in even partially cloudy conditions, whereas deep-sky observational imaging demands long stretches of clear sky.

A common measurement used by observatories is the percentage of photometric nights. The classical definition of a photometric night is for when at least 6 continuous hours of the sky being clear down to 5° above the horizon occurs during the period the sun is at least 18° below the horizon [7] . Another is the percentage of spectroscopic nights. Definitions of spectroscopic nights vary more so than photometric, here the definition adopted will be 65% cloud cover or less (either percentage of sky covered by clouds, or percentage of time covered) for at least 5 hours [8]. By this definition all photometric nights are also included as spectroscopic nights.

Although many observatories have an all-sky camera for monitoring sky conditions, due to the large difference in sensor/lens combinations there is currently no standard automated process for using the data from all-sky camera for site characterisation. As a result the data used in the generation of statistics on photometric nights is still gathered from visual observations recorded in night-time logs by the telescope user [9]. I could find no references to these all-sky cameras being quantifiably monitored for measuring sky conditions, but rather as an aid to visually detecting thin cirrus cloud which is hard to do with the naked eye from dark sites.

Site characterisation is most often used by large astronomical sites when used as the reasoning for locating a new telescope there, and as such these sites are in parts of the world where there are a far greater percentage of photometric nights than in Britain. Although comparing the number of classically photometric nights is interesting, a more appropriate statistic will be needed for the comparison of sites such as Bayfordbury where clouds are present for the majority of the time.

One of the other most important statistics for observing sites is the atmospheric seeing, and one of the main reasons for the situation of large observing sites in high dry locations where the atmosphere is thinner and still. Unfortunately due to the nature of the wide angle lens on the camera, and low resolution of the sensor, the smallest detectable angular size is 18 arcminutes which rules out the possibility of using the camera to measure and monitor seeing conditions.

Images were analysed daily from 30th October 2009 to 27th April 2010, from 4pm to 8am taken at 10 second to 3 minute intervals. Data from 14.4% of all possible nights was either missing or unavailable due to problems with the main computer, primarily during November.

Star Counting Method

The first method attempted to quantify the amount of clear sky was to count the number of stars in each image and then divide this by the number of stars that would be detectable if there were no clouds.

This was done semi-automatically by loading each image in turn into a command line version of the astronomical image processing software Iris [10]. Iris was chosen as of the software initially tried, it had the shortest computational time for the number of stars detected, and its command line interface allowed automation to be more possible.

To begin with a PHP program was written and run to generate a text file program that Iris could then run, this simply involved collating the list of files to be analysed and inserting the FINDSTAR command and parameters. This command detects all stars having a level greater than a given sigma times the level of the sky background noise. A variety of values for sigma were trialled to find the one that detected the most number of stars, and the least number of erroneous results as small patchy clouds were also often detected. The list of detected stars was outputted to a text file along with their full width half maximum. Another program written in PHP then continuously read the text file as it was produced by Iris and disregarding any 'stars' with a FWHM greater than 5 (objects such as smalls clouds, lens flare from the moon, or small plane trails) and then saved the number of stars in each image to another text file. This was then loaded into Microsoft Excel for analysis.

As the resolution in time of the values was much greater than needed (30 seconds or less) the values were averaged as a moving average over 10 minutes by taking the minimum value over this range. This would take into account that passing cloud over such a small time is likely to interrupt an observation and that only a period of at least 10 minutes of clear or partially clear sky will be useful to an astronomer. To calculate the percentage of clear sky each value corresponded to the number of detected stars were divided at first by the maximum number detected, which was 26. However it was noticed that with such a low number of stars the number of detectable bright stars was likely to vary by a significant amount over the course of the night. To account for this a simulation of the night sky with the same field of view and magnitude limit as the camera was created for each degree change in local sidereal time. These 360 simulated images were then run through the program and the results plotted.

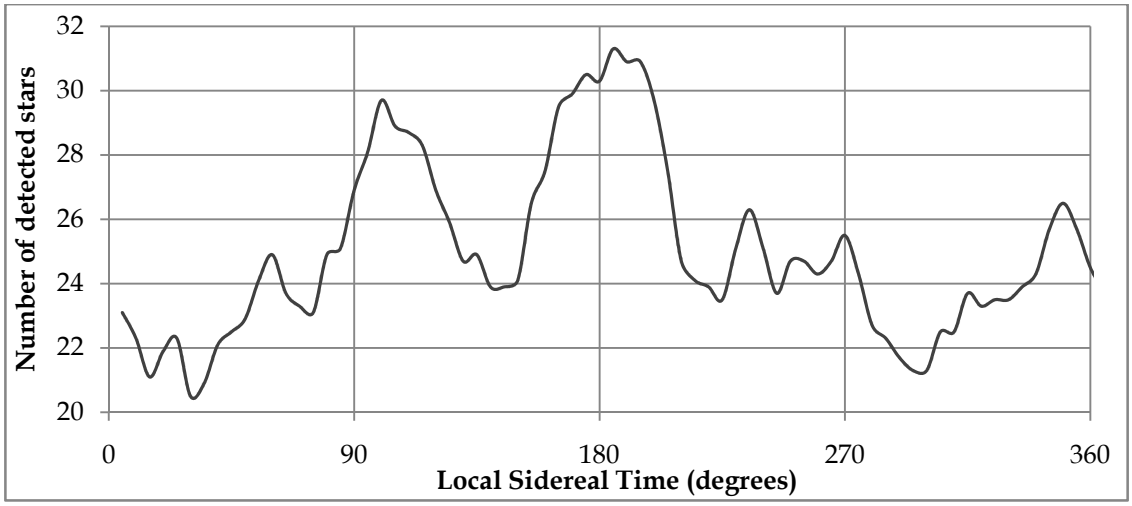

Figure 9: The number of stars detected in a simulated image of the same view of the sky as the camera, at 1 degree intervals. The large amount of variance in successive measurements in relation to the number of stars detected is an indicator of the inaccuracy in the software routine as a method of measuring the total number of stars above a certain threshold.

Figure 9 shows the results of the simulated sky as a function of local sidereal time. An approximate function of two superimposing sine waves was fitted to the curve as they would be periodic over the 360° interval, and proved a reasonable fit.

$$N = 4\,sin\left(4\left(LST - \frac{2\pi}{5}\right)\right) + \left(2\,sin\left(LST - \frac{2\pi}{7}\right)\right) + 25 \quad Eq.\ 2$$

Using the time and date of each image the local sidereal time at that value could then be computed, and from that the number of theoretically detectable stars at that time using the above equation. This then allowed a more accurate value for the percentage of clear sky to be plotted against the time. The difference can be seen in Figure 10, at points it is minimal, at others it can be over 14%.

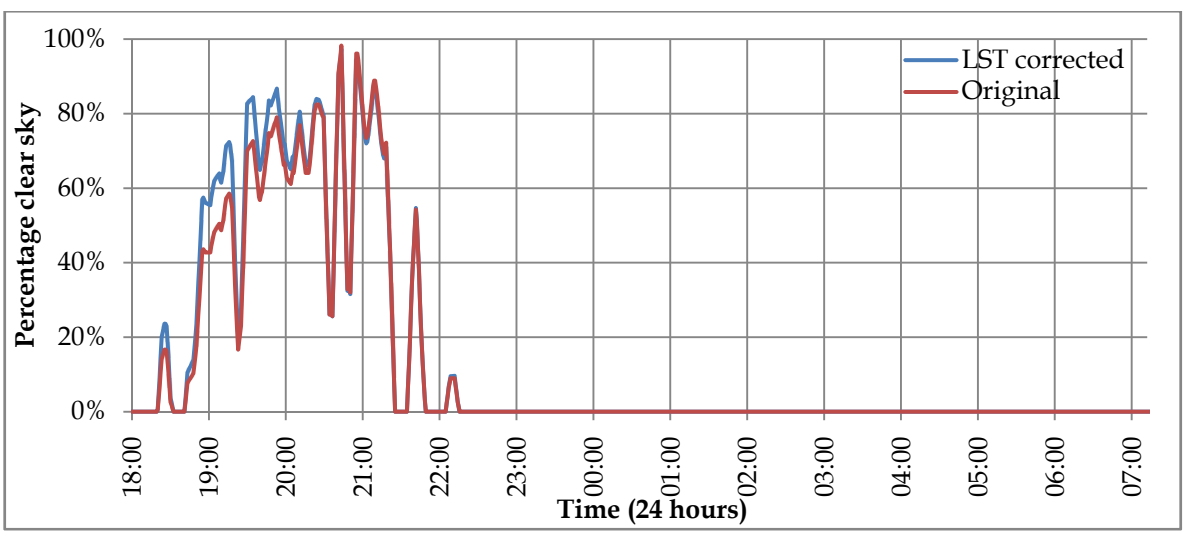

Figure 10: The effect of the inclusion of the theoretical maximum number of detectable stars as the basis of the percentage clear sky calculations. On this particular night (7 November 2009) the difference can see to change with time, with the maximum difference at around 19:00 being over 14%.

This method was soon abandoned as a number of reasons made it unsuitable. The number of stars detected in successive frames could vary by up to 50% despite both being completely cloudless and having almost no difference between them. The processing time and amount of user input between stages would also be impractical as it would be need to be completed each day. It was also realised that the number of stars detected in an image does not provide enough information to be able to determine whether the sky was suitable for observing. For example a calculated percentage clear sky of 50% could represent three scenarios; either half of the sky was perfectly clear, that light patchy cloud was covering 50% of the stars across the whole image, or a mist allowed only the 50% brightest stars to be detected. However, only one of these scenarios would represent useful observing conditions.

Manual Method

To overcome the shortcomings of the automated method, a more manual approach was taken to quantify cloud cover. By viewing the 1 to 2 minute animations of the full night's frames, judging cloud cover by eye becomes a simple task. The results are much more accurate than any automated star counting method and can easily compensate for different amounts of Moon glow, transparency levels in the atmosphere, and small patchy clouds, planes or lens flare from the Moon which are intuitively followed by the eye across the frame.

By viewing the animated video, an estimation of the cloud cover was made by eye. The result was a far more representative value for cloud cover over the night than the star detection method could produce. Despite being completely manual, it took far less time to complete - only slightly longer than the length of the video – around 3 minutes, compared with the half hour or longer for the automated method.

In order to visually quantify the fraction of clear sky the metrological system of oktas (or eighths) cloud cover was used, where 0 oktas indicates totally clear sky, and 8 oktas represents totally overcast [11]. This is also regularly used in observatory night-time logs. Whilst viewing the video the average okta values over hour intervals from 4pm to 8am each night were recorded. Two values were then calculated for quantifying the entire night; the first is the integrated clear sky percentage, calculated by averaging the okta values for the night and dividing by 8 to express it as a percentage. The second is the total hours of useful clear sky for the night, a sum of hours with values of 0 or 1 oktas. Nights containing 6 consecutive hours of 0 or 1 oktas between astronomical sunset and sunrise are classed as photometric. Those with 5 or more hours of 5 oktas or less between sunrise and sunset are classed as spectroscopic.

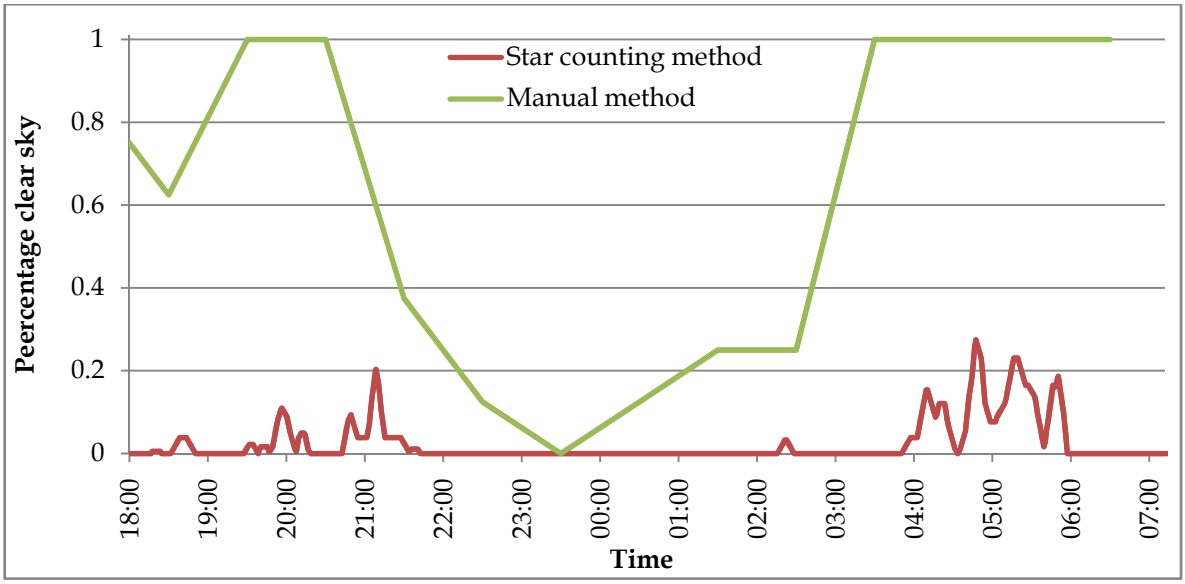

Figure 11: The difference between the first automated method, and the second visually estimated method. On this particular date (3 November 2009) the Moon was over 99% illuminated and above the horizon all night. As a result even when the sky was completely clear, the software in some cases detected no stars due to the increased background and shortened exposure times.

As can be seen in Figure 11, in the worst case scenario where an almost full Moon was visible throughout the night the fully automated method failed to produce useful results. Although the correlation can be seen, the large variance even at times of total clear sky and non-detection of any stars at some points despite them being visible rules out the possibility of simply scaling up the automated method's results. No doubt a more thorough and dedicated automated program could be created in the future capable of accurately measuring the cloud cover. More success may be attained by using an algorithm to detect the clouds by pixel values, rather than trying to detect the stars. This will be far less affected by the Moon; otherwise the Moon's phase, altitude as well as atmospheric clarity would have to be factored into star detection.

An important advantage of the manual method is its intuitive nature. The method of using oktas to measure cloud cover is widely used for this reason, including the users of many observatories as they record sky conditions in the night-time logs. Anyone wishing to perform similar analysis using the camera in the future will easily be able to follow this method and produce useful comparative results, much more so than the first method.

Histogram analysis method

A third and final method was developed for estimating cloud cover in images, designed from the start to run continuously and autonomously on the computer running the camera.

This method analyses a histogram of the counts of different pixel values (0-255) in each image and calculates 5 parameters based on the shape of the histogram, which are then combined with a small correction for the effects of moonlight to estimate the cloud cover.

A program was written in PHP to visualise the histogram of a given image to allow images to easily be analysed when developing the idea. To reduce noise the pixel values were binned 2x so the range was reduced to 0-127. The histogram outputs of several images with a range of cloud cover are shown below, alongside their respective images.

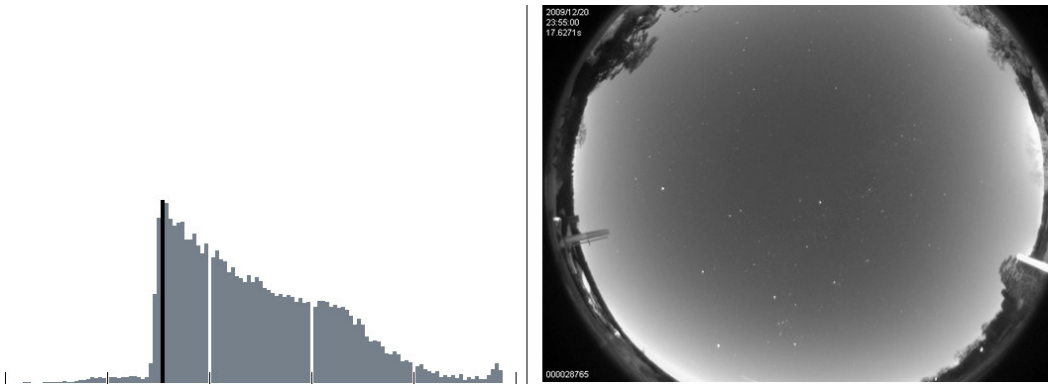

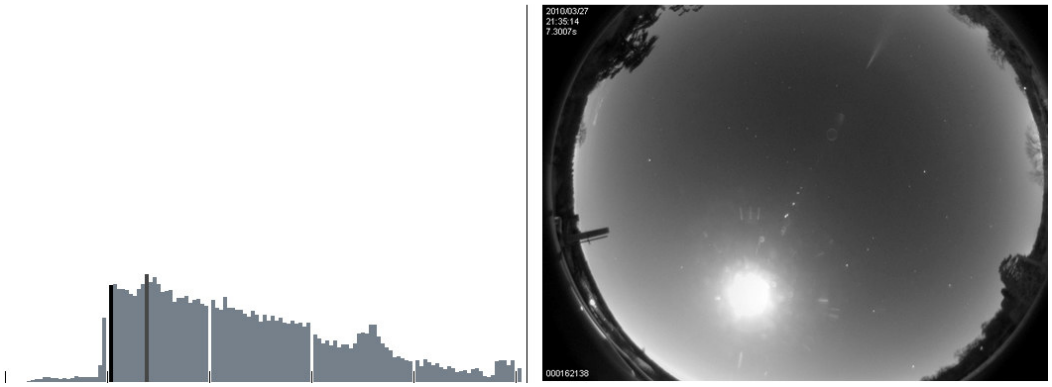

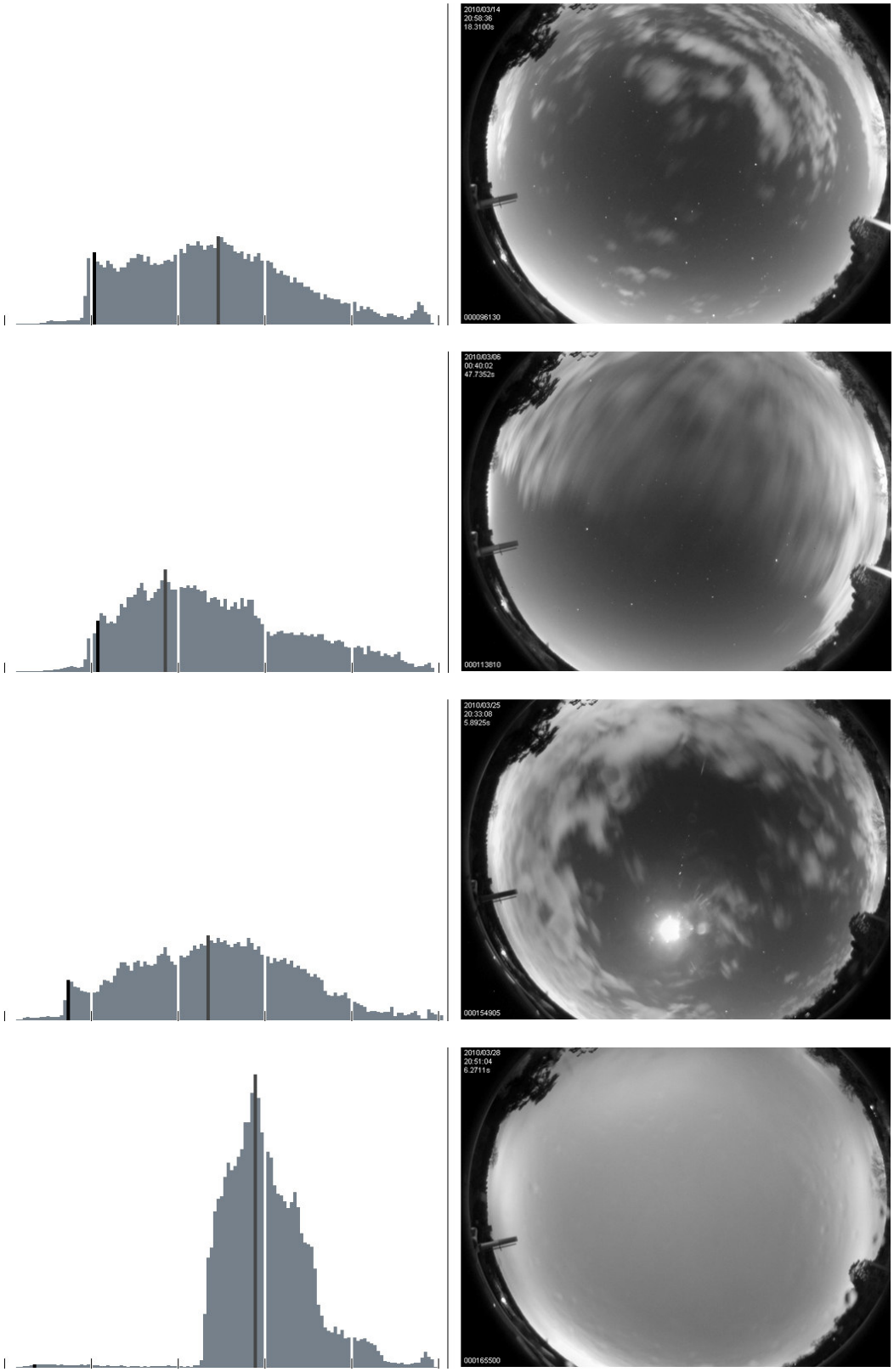

Figure 12: A range of images with their tonal histograms. Markers represent each set of 25 pixel values, the black bar indicates the value of the maximum positive gradient, and the dark grey bar indicates the pixel value with the maximum number of counts in the image.

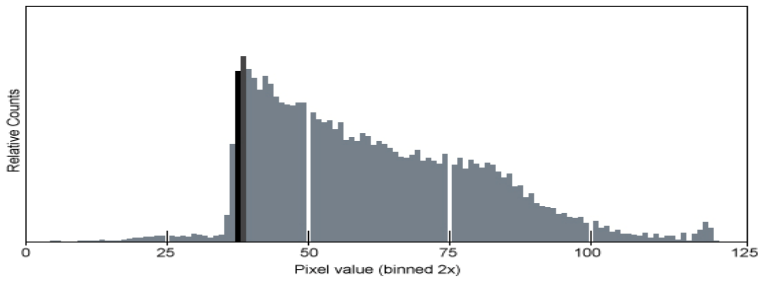

Figure 13: The annotated histogram of a typical clear sky image. It is easy to see the near-triangular profile of an ideal cloudless image with the steep rise between the surrounding black frame and the dark sky background in the centre, which then descends very linearly away as it follows to gradient of the sky towards the horizon.

Parameters:

$\tau =$ The largest positive gradient between two points 3 pixel values apart on the histogram. This value is the single best parameter for indicating percentage cloud cover. Its value ranges from close to 100 for perfect conditions, down to 0.5 for overcast skies.

$\alpha =$ The ratio between the counts at pixel value 75 and the point of maximum gradient. Due to the uniform slope on a clear sky histogram, this should be around 0.5 but increase dramatically to upwards of 70 for very smooth overcast clouds.

$\beta =$ The difference in pixel values between the point of maximum gradient, and the point of maximum counts. For clear sky this should be very small, 1 or 0, but can increase to upwards of 60 for overcast conditions.

$\gamma =$ The ratio between the counts of the maximum, and the counts of the point of maximum gradient. Clear skies would give a value close to 1, but an increase would signal a peak away from the first gradient rise, indicative of cloudy conditions.

$\varepsilon =$ The sum of deviations of each pixel value from a line drawn between the top of the point of maximum gradient and zero at pixel value 105. An ideal noiseless clear sky image would give a value approaching zero, and increases to over 5 for overcast skies. This value is useful for identifying most dark clouds, which can give a similar profile to clear skies with a large maximum gradient and no further peak. This deviation parameter however accounts for the non-uniform nature of the overcast sky.

$\varphi =$ The sum of the differences of the counts of a pixel value and that of the pixel value 2 higher, taken over the range of 50 pixel values after the point of maximum gradient. Certain particularly dark clouds may give a profile very similar to that of clear sky when covering the entire sky using the first five parameters. This value detects more subtle irregularities in the slope of the line than parameter ε. Whilst the gradient of a clear sky is very uniform and so differences between successive pixel values are small, overcast conditions almost always present a non-uniform appearance, and so this value can differentiate between the two with far better accuracy. For clear skies this parameter has a value of below 4, and typically above 8 for cloudy conditions.

Accounting for the Moon

We have already seen how the effects of moonlight can cause problems when calculating the amount of clouds in the images. Unlike the star-detection method which falls apart completely when the moon is up - even during totally clear skies, this method is less affected to the extent that almost no correction is needed during clear skies. However during partial cloud the moon has an amplifying effect on the clouds by increasing the brightness level.

To correct for this a 'moon brightness factor' μ was calculated which has a value between 1 and 0, where 1 would be a 100% full moon at the zenith. The perceived brightness is dominated by two effects, the phase of the moon, and the altitude above the horizon.

The phase angle of the moon is calculated using the low accuracy formula given by J. Meeus [5] based on the sun and moon's mean anomaly and the mean elongation of the moon. If x is the cosine of the phase angle then by fitting a curve to values given by K. Long [12] the natural log of the relative brightness due to the phase of the moon is given by ω:

$$\boldsymbol{\omega = 1.0524x^3 - 0.2837x^2 + 1.7291x - 2.5} \qquad \textit{Eq. 3}$$

The right ascension and declination of the moon were calculated using the reduced form of the Chapront ELP2000/82 lunar theory given by J. Meeus [5]. If H is the local hour angle of the moon (the local sidereal time minus the right ascension), δ is the declination, and φ is the geographical latitude of the camera, then the sine of the moon's altitude h is given by Eq. 4 [5]:

$$\boldsymbol{sin(h) = sin\,\varphi\, sin\delta + cos\varphi\, cos\delta\, cosH} \quad \textit{Eq. 4}$$

The affect of atmospheric extinction on the original intensity as a function of altitude is then given by Eq. 5 where c~0.2 for visible wavelengths [13]:

$$\boldsymbol{I = I_0 e^{\frac{-c}{sin\,(h)}}} \qquad \textit{Eq. 5}$$

Multiplying the phase and extinction factors together gives the overall 'brightness factor' μ as a function of the phase and altitude:

$$\boldsymbol{\mu = 1.221 e^{\left(\omega - \frac{0.2}{sin\,(h)}\right)}} \qquad \textit{Eq. 6}$$

Calculating the final okta value

The calculated values of each parameter were plotted on a graph for each frame number, as well as a manual analysis for reference. Each parameter was then normalised to give the best fit over the manual reference line. The normalised values were then combined in a weighted average to give the best overall fit. The final formula for the okta value of cloud covering the sky is given in Eq.7:

$$\boldsymbol{1.2\left(2\alpha^2 + \frac{\beta}{16} + 2.5\gamma + \varepsilon + \frac{500}{\tau^{3/2}} - \varphi - \sqrt{2\mu} - \mu^2 - 5\right)^{3/4}} \quad \textit{Eq. 7}$$

The resultant value must be clipped between the values of 0 and 8, and finally averaged over 15 frames (typically 5 minutes worth) to smooth out any anomalous values.

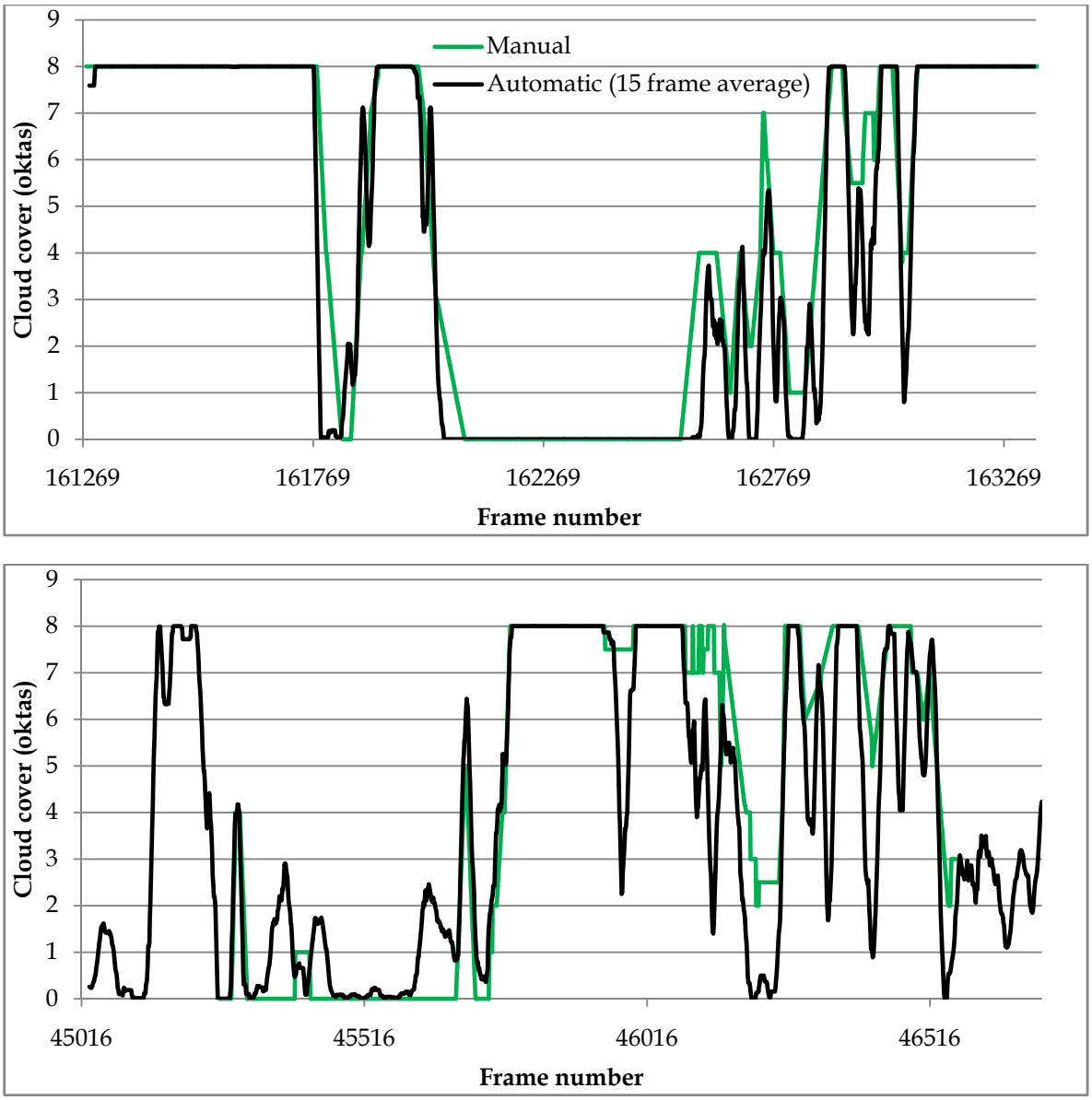

Figure 14: Two plots of cloud cover fractions calculated using the automated method given in Eq. 7 (black line) and approximate manual estimations (green line). An obvious correlation can be seen, although not perfect.

When used to calculate the hourly clear sky data for each night as with the manual method, the histogram analysis method was in good correlation with the manual results. Over the period of 15th March 2010 to 15th April 2010 where the most consistent images were taken after the resolution of computer difficulties, the average difference in values of the total integrated percentage was 6.5% and the average differences in total number of clear sky hours was 0.7. Neither method can be taken as being absolute, as the histogram analysis gives a perfect integration over time, whilst the manual method is less accurate at this being human judgement but the estimation of the clouded fraction by eye in certain circumstances cannot be surpassed by the automatic method.

Results

I see two main uses for the results of sky condition analysis. Firstly for the site characterisation of Bayfordbury observatory, and being able to compare conditions here using standard measurements to other sites both in the UK and abroad. Secondly to examine if any patterns in local weather conditions can be detected that may benefit anyone planning on using the observatory.

The data used to produce the results was taken using the manual method, as this has been completely analysed by eye it is deemed the most reliable.

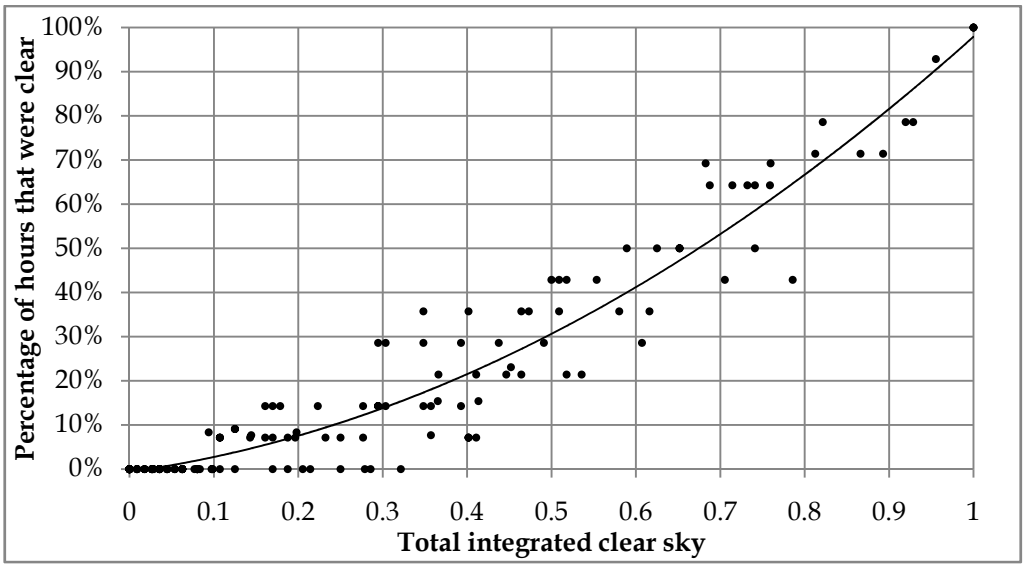

Figure 15: This shows the correlation between the two values for each night calculated to quantify the amount of clear sky. The correlation is very strong, with a Pearson product-moment correlation coefficient of 0.94.

To start, the correlation between the two calculated values for each night is plotted in Figure 15. The points follow very closely to a second-order polynomial trend-line. As the total integrated clear sky value for a night does not differentiate between a night where the sky is clear for the first half and totally cloudy for the rest, or one where the sky is half covered with cloud for the entire duration of the night, this is quite a surprising result. It can be seen that where the total integrated value for a night is above 32%, there has always been at least one full hour of clear sky despite it being possible using the method employed for the average total integrated value over one night to reach 75% without a single hour of clear sky. This indicates a strong tendency not to be partially cloudy for long periods of time.

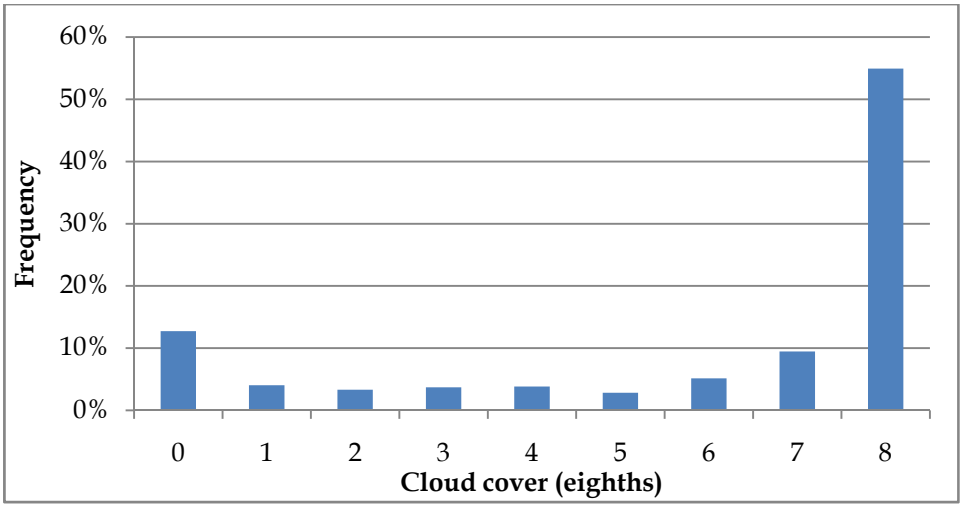

Figure 16: The frequency distribution of all hourly cloud cover measurements. 64% of recorded hours had near or complete cloud cover, whilst useful clear hours (0 or 1 oktas) accounted for 17%. Partially cloudy conditions (2-6 oktas) accounted for just 19%.

This conclusion is reinforced by the results of Figure 16 which shows that although largely clear or overcast conditions represent half of the possible values; they represent 81% of the frequency distribution. Periods of 2-6 oktas cloud cover usually occur during transitions between clear and overcast skies, and rarely occur for periods of more than 5 hours at a time.

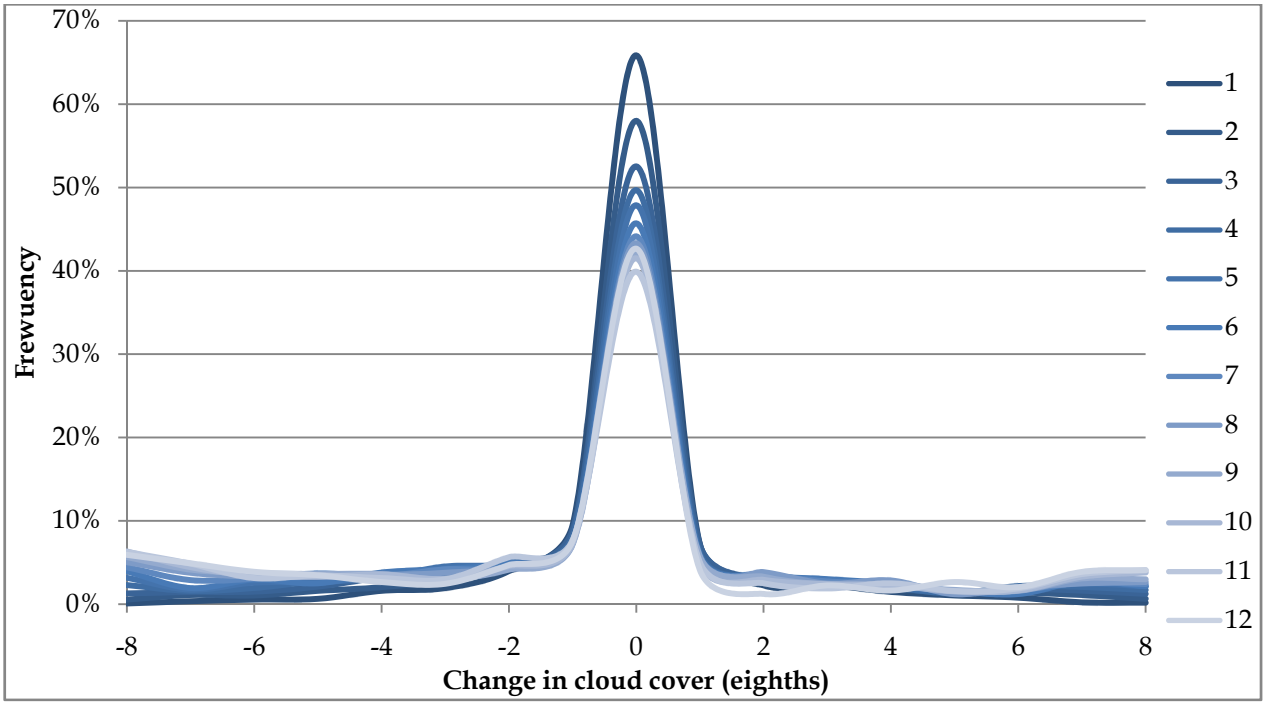

Figure 17: The frequency distributions of the changes in cloud cover after a given number of hours. The tendency not to change can be seen, as there is a 66% chance the cloud cover will remain the same after 1 hour, which drops by just 26% after 12 hours.

The tendency to not change is further demonstrated in Figure 17, which shows that by far the most frequent occurrence is for subsequent hours to remain the same in terms of cloud cover. Either side of no change there is not a large difference between increasing and decreasing values, but after 8 hours there is a slight increased tendency to change by larger (6-8 eighths) rather than small amounts.

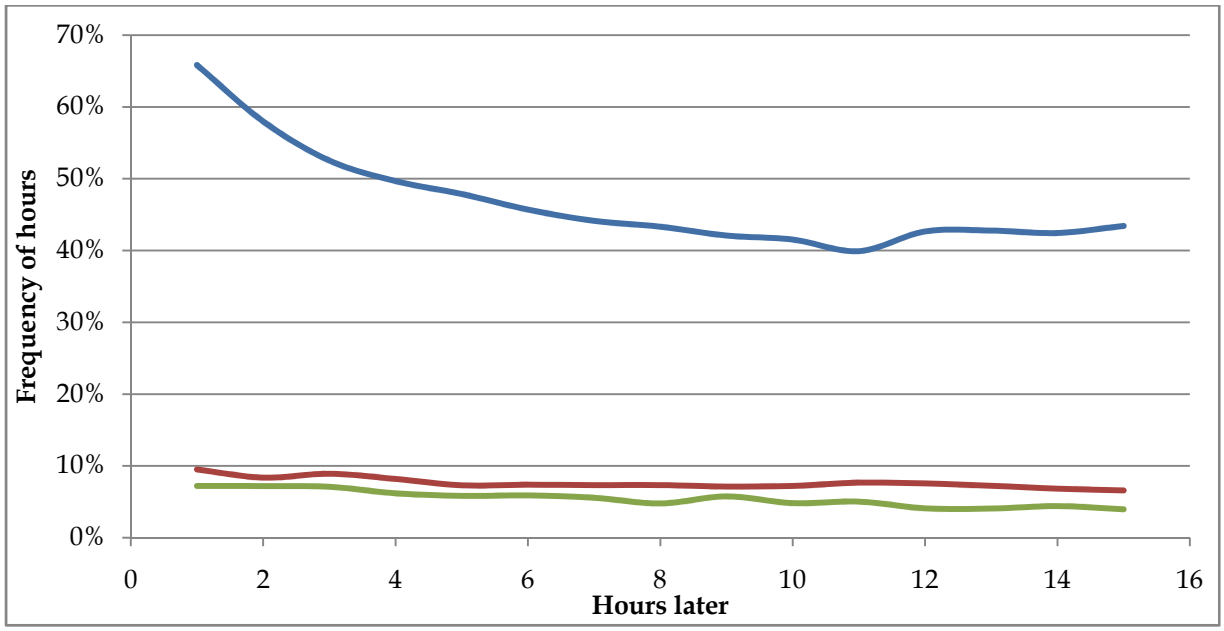

Figure 18: The frequency in which a change of cloud cover occurs after a certain number of hours. Changes of 0 (no change), -1 (one eighth less cloud cover) and +1 (one eighth more cloud cover) are shown.

This is further observed in Figure 18 where the 3 most frequent changes (0, -1 and +1 oktas) are plotted as a frequency of occurrence after a certain number of hours. The likelihood of one eighth increase in cloud cover barely changes over time, whilst there is a small increased chance of cloud clearing after 10 hours. There is also a constant (9.8% average) increase in likelihood to get clearer over the night than to get cloudier. This would indicate that more clouds are created during the day as the masses of water are warmed by the Sun, and are less likely to form or more likely to dissipate during the cooler nights. As with Figure 17 it clearly shows that by far it is most likely for cloud cover to remain the same during consecutive hours, dropping from 66% after 1 hour to no less than 40% even after 12 or more hours.

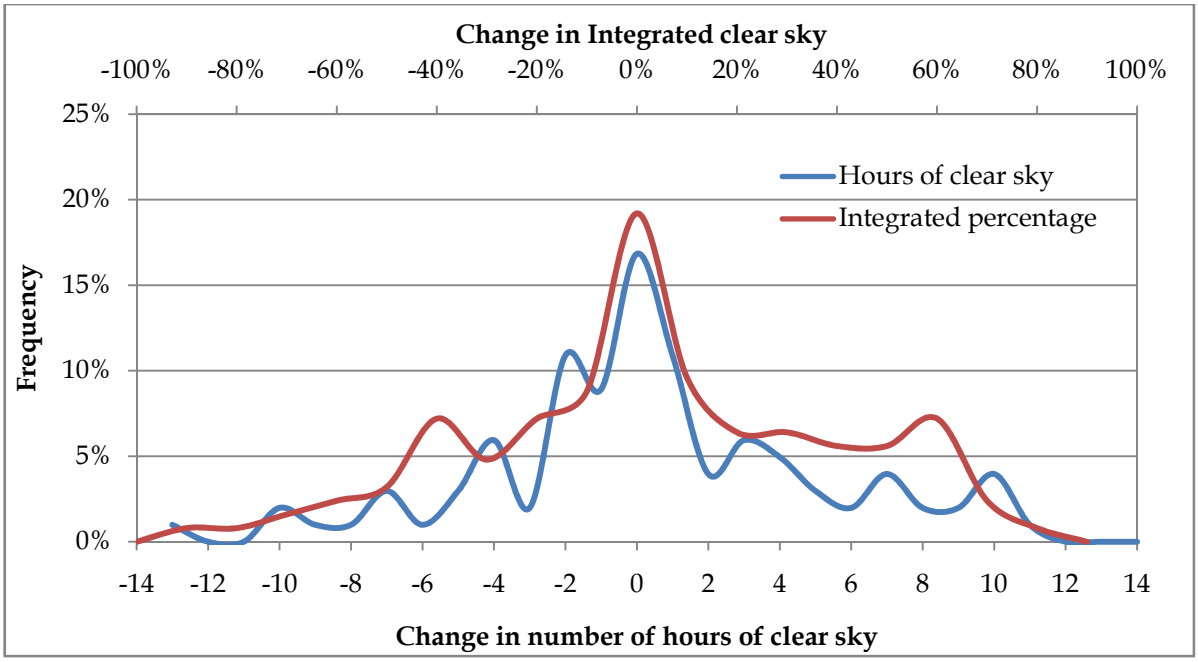

Figure 19: Similar to Figure 17, this frequency distribution shows by how much the weather is likely to change, but across consecutive nights. Two values are plotted, the change in number of hours of clear sky for the following night, and the change in the integrated clear sky percentage.

When examined over longer timescales the trend still persists. In Figure 19 where cloud cover is compared to the following night, the tendency again is seen for the weather not to change as both graphs peak at the point of no change. However in this case the majority is much smaller, being only a 19% change of the next night having similar integrated percentages, and a slightly lower chance of having the same number of hours of clear sky.

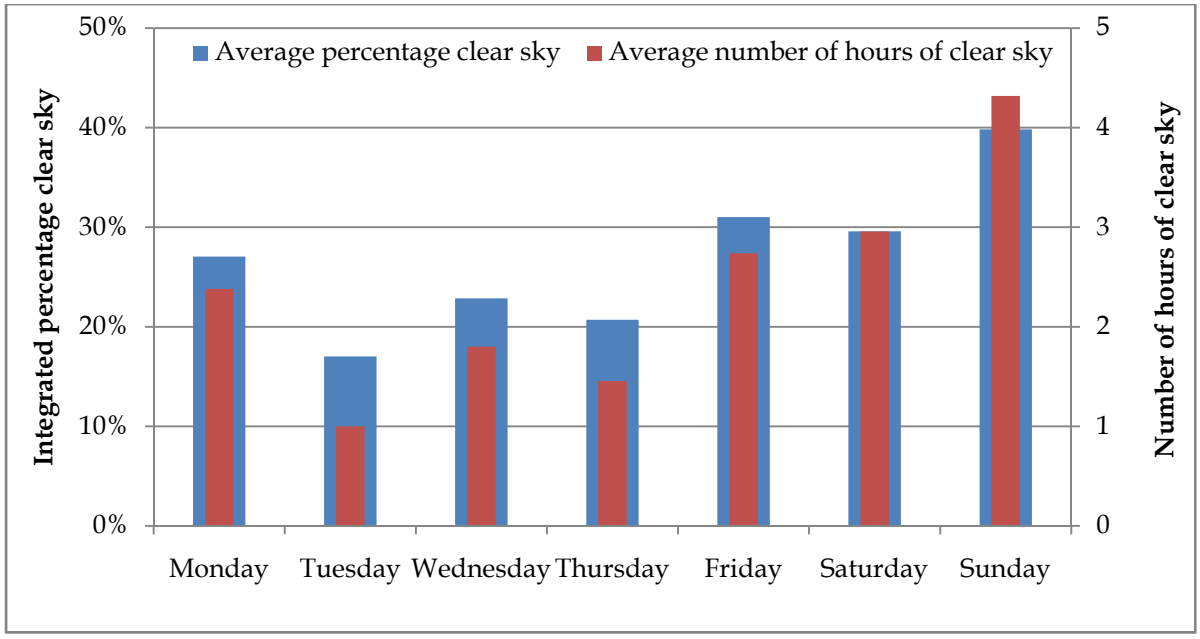

Figure 20: For each night of the week the average values for the integrated percentage clear sky, and the number of hours of clear sky were calculated and plotted. The correlation between the two can be seen.

Interestingly, there is a very large difference between the average cloud cover on different days of the week, the average difference between the clearest and cloudiest days (Sundays and Tuesdays) is 22.8%, or 3.3 more hours of clear sky per night. As the week is a man-made concept and so is uninfluenced by natural causes, any actual differences must be down to human causes such as industrial or traffic emissions. Further measurements would be needed to see if error bars reduce or the difference between different days increases to know conclusively if the difference is an actual one.

Day\hour	17-18	18-19	19-20	20-21	21-22	22-23	23-00	00-01	01-02	02-03	03-04	04-05	05-06	06-07
Mon	14.3%	10.0%	15.0%	20.0%	25.0%	25.0%	20.0%	31.6%	15.8%	11.1%	16.7%	16.7%	22.2%	20.0%
Tue	23.8%	9.5%	4.5%	4.5%	0.0%	0.0%	9.1%	4.5%	4.5%	4.5%	9.1%	9.1%	9.1%	9.1%
Wed	10.5%	11.1%	11.1%	15.8%	10.5%	21.1%	10.5%	5.3%	10.5%	5.3%	21.1%	21.1%	16.7%	18.8%
Thu	17.6%	26.3%	15.8%	15.0%	19.0%	9.5%	9.5%	14.3%	9.5%	4.8%	0.0%	14.3%	4.8%	10.0%
Fri	38.1%	23.8%	28.6%	31.8%	18.2%	18.2%	22.7%	18.2%	13.6%	18.2%	22.7%	13.6%	9.1%	4.8%
Sat	17.4%	21.7%	26.1%	21.7%	26.1%	21.7%	17.4%	21.7%	17.4%	21.7%	21.7%	21.7%	26.1%	21.7%
Sun	28.6%	47.6%	47.6%	47.6%	42.9%	42.9%	38.1%	23.8%	14.3%	5.0%	10.0%	25.0%	28.6%	30.0%

Table 1: A more thorough breakdown of Figure 20, by further splitting each day into hour intervals. The percentage values shown were calculated by dividing the total number of hours for each hour/day combination that were clear, by the total number of hours evaluated.

From Table 1 we see that averaging over the days of the week gives us insufficient information. Most prominently on Sundays, which have the highest overall average clear sky value, whilst clear between 6pm and 11pm for almost half of hours recorded, are rarely clear between the hours of 1am and 4am.

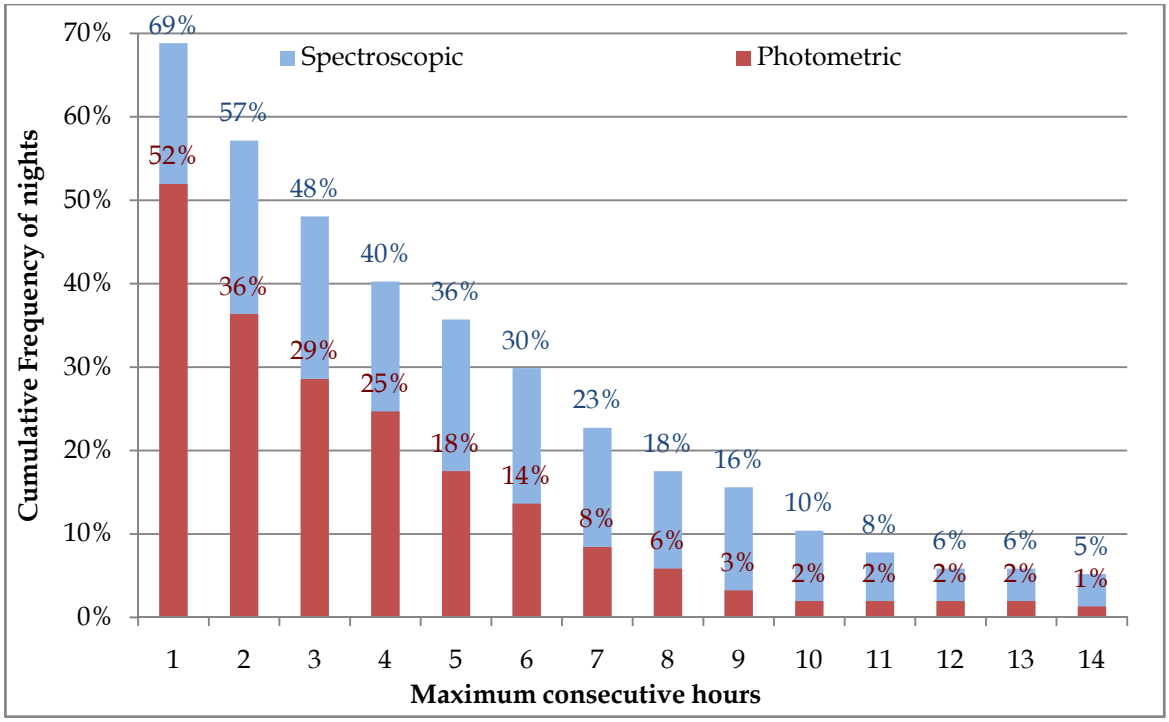

Figure 21: The cumulative frequency of nights containing hours of photometric or spectroscopic skies. 46.3% of nights contain at least one hour of photometric sky, and 68.8% contain at least one hour of spectroscopic sky.

Using the classical definition of a photometric night, a value of 13.6% of nights recorded were deemed photometric (21 out of 154) – almost an average of one per week, and 35.7% were spectroscopic (55 out of 154) – and average of 2.5 per week. 18.8% of nights were completely overcast from sunset until sunrise, and 48.0% of nights had no whole hours of photometric sky. Of all hours recorded, 16.8% were photometric, 18.8% were spectroscopic, whilst 64.4% were overcast.

	Bayfordbury (England)	**San Pedro Mártir (Mexico)**	**Mt. Graham (Arizona, USA)**	**Mauna Kea (Hawaii, USA)**	**La Silla (Chile)**	**La Palma (Canary Islands)**
Photometric	12.6%	56.6% [2]	41% [2]	48% [2]	59.8% [2]	51.7% [6]
Spectroscopic	35.7%	80.4% [2]	58% [2]	69% [2]	82.2% [2]	

Table 2: A comparison of the percentage of photometric and spectroscopic nights between Bayfordbury and some of the world's top observing sites.

From Table 2 we see that over the period recorded Bayfordbury typically has around 20-30% the amount of photometric nights, and 45-60% the amount of spectroscopic nights in comparison to top observing sites. The sample of nights analysed is however biased as it was recorded over the winter and early spring months. In the case of the locations compared above, the percentage of photometric nights available has been seen to vary by over 40% from summer to winter [8].

3) Variable Stars

Mira type variable stars are cool red giant stars, which vary in brightness dramatically over the course of hundreds of days. Their namesake, Mira (o Ceti), is the brightest Mira variable, and at its brightest can peak at magnitude 2.0 before dipping well below naked eye visibility to magnitude 10.1 [15].

Due to their large variation in brightness, and long timescales between maxima and minima, their variation should be detectable over long periods. As the camera will be in continual operation, every clear night will be recorded and present the opportunity to record a data point to add to a light curve.

A number of stars identified using previous light curves to determine the suitability for observations are given in Table 3. Their suitability is based on their maximum brightness being above the limiting magnitude threshold of magnitude 5, having their maxima peak during the period of observation (November 2009 to May 2010), and also that they are visible from Bayfordbury during night-time hours during their maximum period.

Star	**Maximum Magnitude**	**Minimum Magnitude**	**Period**	**Estimated Peak**	**Transiting altitude**	**Visibility**
o Cet (Mira)	2.0	10.1	332 days	15 Nov 2009	35.2°	Until mid January
χ Cyg	3.3	14.2	408 days	15 Dec 2009	No transit	Until mid December
R Leo	4.4	11.3	310 days	15 Sep 2009	49.5°	Duration of project
U Ori	4.8	13.0	368 days	15 Mar 2010	58.4	Duration of project
R Cas	4.7	13.5	430 days	01 Mar 2010	89.5	Until mid March
α Her	2.74	4.0	Irregular	-	No Transit	Before Dec/After Jan
R Lyr	3.88	5.0	46 days	-	No Transit	Until mid December

Table 3: List of potential candidate variable stars to detect over the period of observations (15).

In reality, even these most suitable stars were not as possible to detect as previously imagined. One reason being that although their maximum brightness may be within the grasp of the camera, successive maximum brightness themselves have variability, and there is no guarantee that any maximum will be bright enough to be visible. Additionally the background gradient of the sky due to surround light pollution swamped out dimmer stars with a lower altitude, as well as making accurate photometry much more difficult.

In fact only one star from the list in Table 3 was able to be accurately identified and measurements made of it, and that was Mira itself. Even so, the strong background gradient was a challenge to remove before being able to perform photometry.

In addition, only 4 nights during the time that Mira was visible (November-Mid January) were clear and moonless enough. Those nights that were measured however once calibrated do fit in with confirmed observations taking by the American Association of Variable star observers as shown in Figure 22:

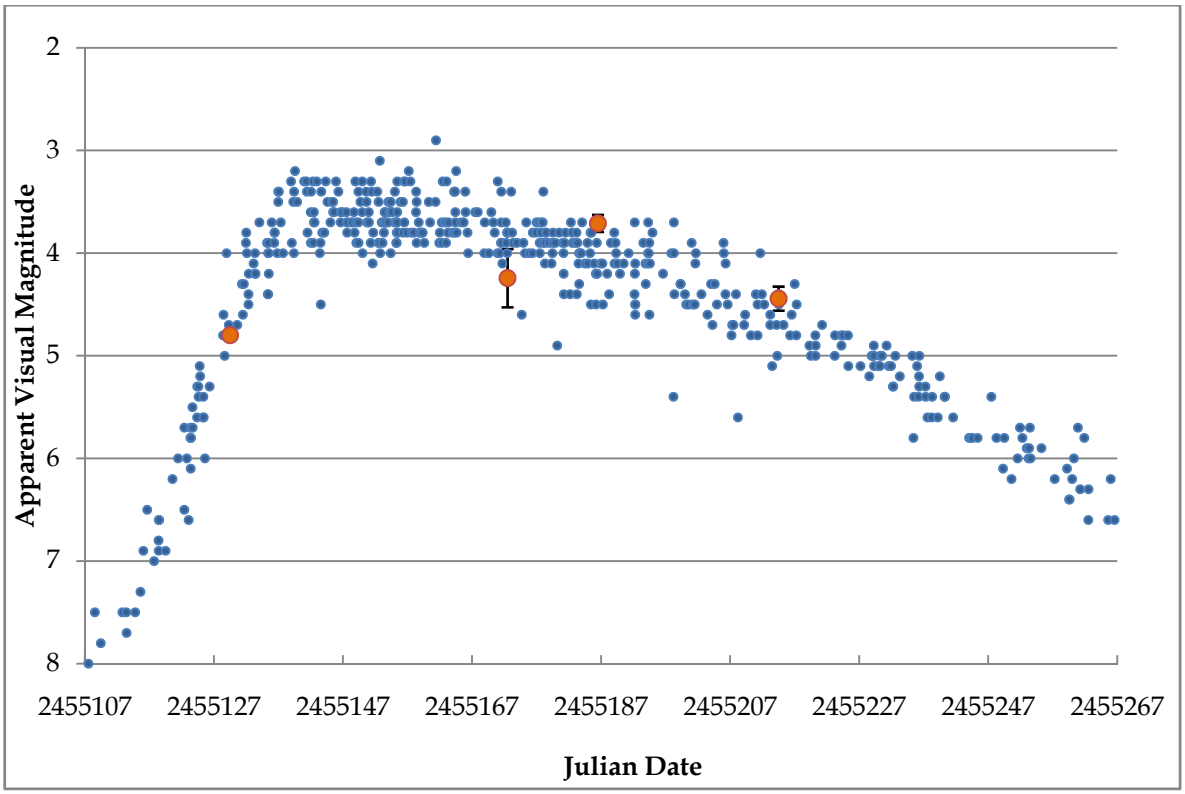

Figure 22: The light curve of o Cet (Mira) during its maxima period in November 2009. Measurements obtained from the camera are plotted in orange, and observations from the American Association of Variable Stars Observers [15] plotted in blue.

4) Transient Events

Meteors

One of the most impressive transient events to an observer at night is a meteor, commonly known as a shooting star. These are the trails of glowing ionised gas created as a particle of debris from space passes through the Earth's atmosphere at several kilometres per second. Typical meteor originators range in size from the size of a grain of sand (1mm) upwards, more massive objects creating increasingly bright trails.

Information on the details of a meteor can be scientifically important for a number of reasons. Details on the frequency of meteors visible during a meteor shower; caused by the Earth's passage through a stream of material left as a comet passed near the sun, can allow the makeup of the stream to be determined and predictions made about future showers.

In the case where a meteor has sufficient mass and composition to survive atmospheric entry and make it to the Earth's surface as a meteorite, details of the objects trajectory may be calculated using accurate observations from multiple sites. This may lead to the recovery of the meteorite and also the calculation of the object's original orbit.

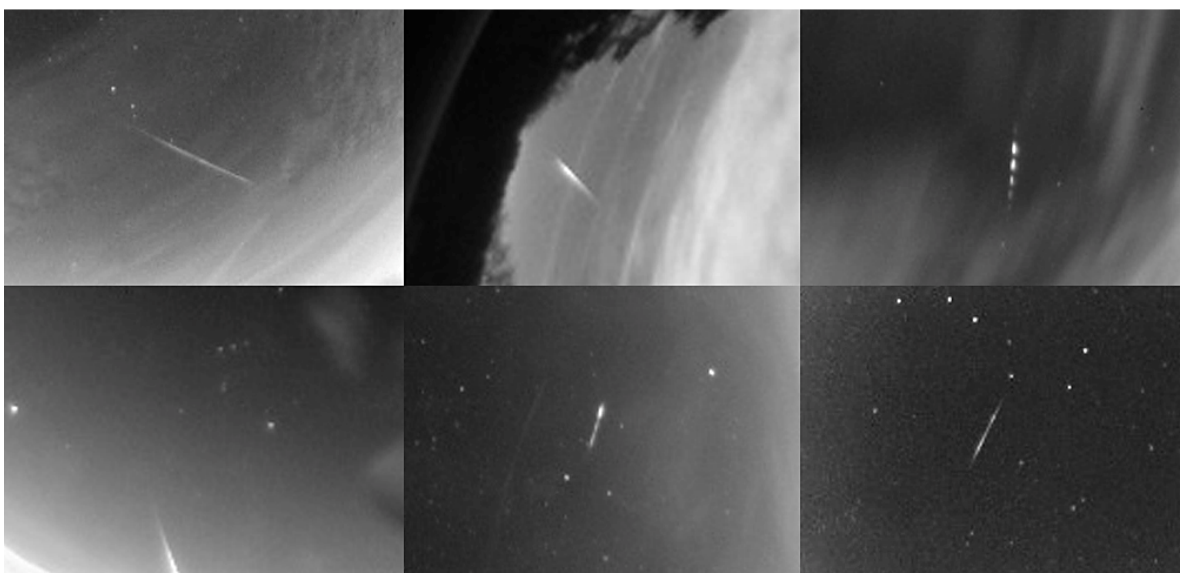

Figure 23: A variety of the brightest suspected meteors over the period analysed. The one in the top right image was captured when testing the 5Hz chopper shutter.

If V is the linear velocity of the meteor, θ is the meteor angle from the radiant, h is the altitude of the meteor, and l is the height above the Earth of the meteor, then its angular speed in degrees per second across the sky is given by ω in Eq. 8: [13].

$$\boldsymbol{\omega} = \frac{\mathbf{180}}{\boldsymbol{\pi}} \frac{\boldsymbol{V sin(\theta) sin(h)}}{\boldsymbol{l}} \qquad \textit{Eq. 8}$$

However for an image of a meteor from the camera, only one of these variables is known; the altitude h. In the case where a meteor can be linked to a particular meteor shower, the angular distance θ between the radiant and the meteor can also be found.

If an object is travelling with angular speed ω, and is captured by a camera with an angular resolution per pixel of R, and the exposure is for a length of t seconds, then the difference in magnitude between the object and one remaining stationary but registering the same number of counts is given by Eq. 9:

$$\boldsymbol{\Delta m = -2.5 log \left(\frac{\omega t}{R}\right)} \qquad \textit{Eq. 9}$$

Knowing that the limiting magnitude for being able to see a star in an unprocessed JPEG image from the camera is around magnitude 5 for a typical 30 second exposure, then the limiting magnitude for a meteor with a range of angular speeds is given in Figure 24:

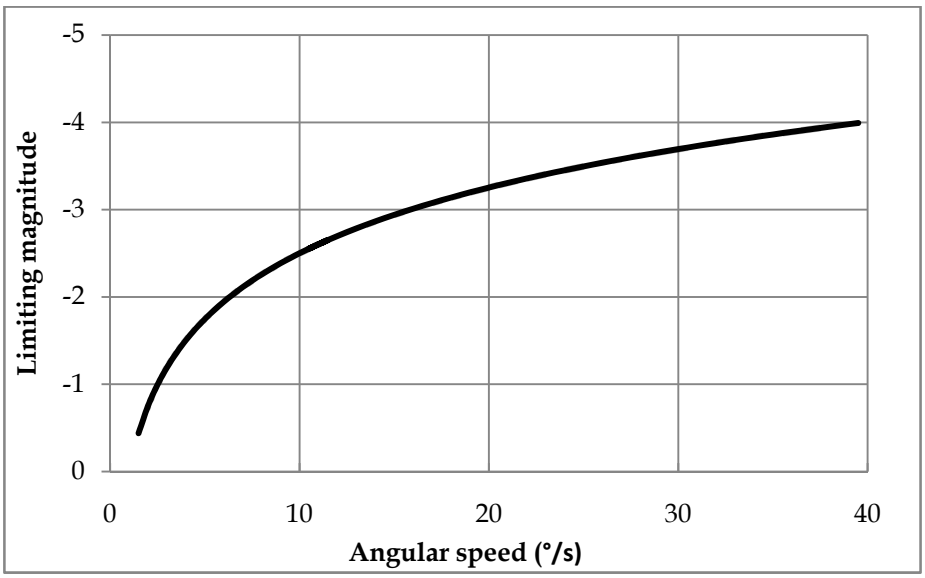

Figure 24: The limiting magnitude of an object travelling with a particular angular speed in a typical unprocessed JPEG image with a 30 second exposure time.

Whilst objects below magnitude 5.5 are detectable in processed FITS images, being able to process and inspect each of the 2000 FITS images for low brightness meteors each night would be a near impossibility. Whereas finding meteors by eye in JPEG images can take only a few minutes per day.

Very low speed (<10°/s) meteors will have to have a larger incoming surface area and hence mass to ionise the air to the same brightness to be visible, and hence lower speed meteors are inherently likely to be brighter. From Figure 24 we can then see that the absolute minimum visible meteor in the images is likely to be brighter than magnitude -1, or more likely above -3. Given that even though the lowest threshold magnitude is visible, only those meteors slightly brighter than this would be noticeable to the eye when scanning through the thousands of frames, it is reasonable to

assume that almost all meteors picked up will have a zenithal magnitude of -3 and above – or classed as fireballs, and are important enough to warrant reporting to the International Meteor Organization Fireball Data Center [16]. Conversely, any meteors of fireball magnitude passing through the field of view of the camera when not cloudy should also be recorded.

The object captured in the top right image in Figure 23 occurred on 6th March 2010 at 03:36:15 ±15 seconds. During this time the 5Hz chopper shutter was running and so the trail is segmented, thus we can calculate the angular speed of the object. 37 pixels (equalling 11.1°) were traversed during 5 segments, or 1 second, giving an angular speed of 11.1°/s, putting it into the speed range of meteors rather than satellites. The non-symmetrical nature of the trail also suggests this. We now have all of the values required to satisfy Eq. 9; ω=11.1°/s, t=27.07s and R=0.3°/pixel. Inserting these values gives a Δm of -7.50. Although the image has a lot of patchy clouds, two bright stars are visible; Vega and Arcturus both with a magnitude of around 0. As the meteor trail is visibly brighter than both, the lower limit estimate for the visual magnitude of the meteor is -7.5. Unfortunately during this period the FITS files were not being recorded due to the problems with the computer, and so accurate photometry cannot be performed.

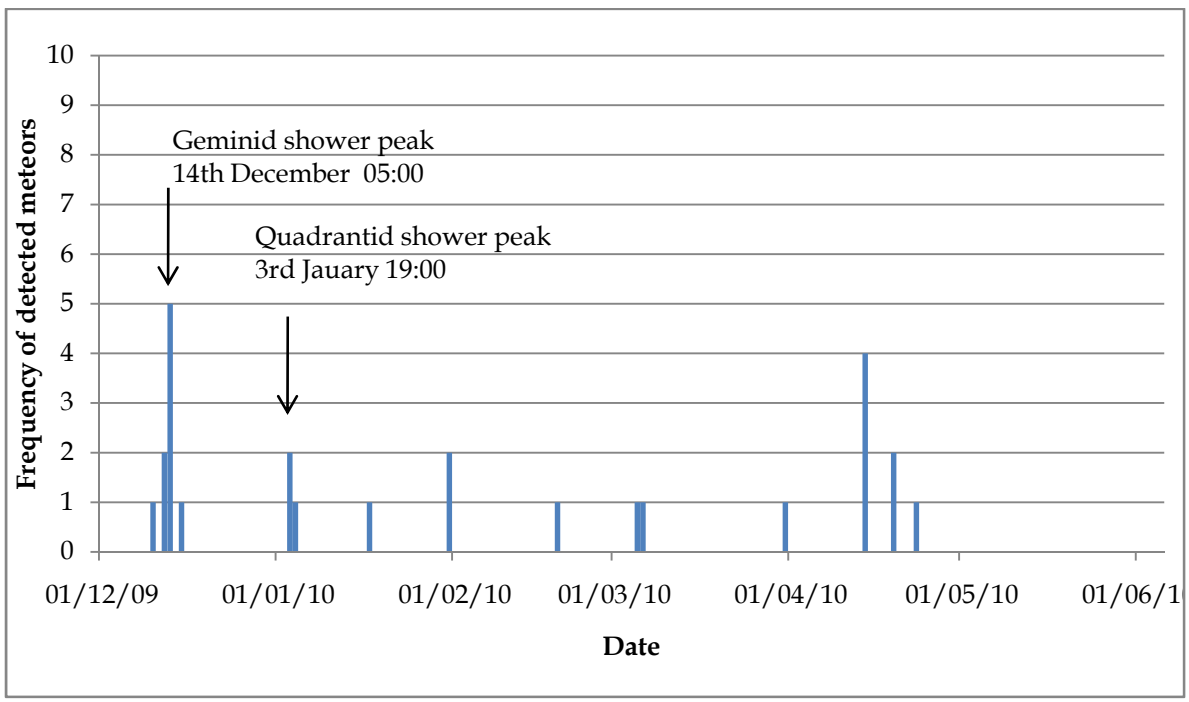

Figure 25: The total number of detected meteors for each night from December 2009 until May 2010

The total number of meteors detected over each night is show in Figure 25, and the peaks of the two most prominent meteor showers to occur over this period, the Geminids and Quadrantids, can be seen to stand out from the surrounding days.

Artificial Satellites

When recording suspected meteors in images they first were matched against a list of known satellite flares, which can give very similar trails.

The most common satellite trails to be picked up by the camera were those belonging to the Iridium communication satellites. These satellites have large polished antennas which reflect sunlight and when travelling over an observer on Earth at the correct angle can be seen to grow in brightness from near-invisible to up to magnitude -8 and fade away again during a period of around 30 seconds [17]. The flares produced by Iridium satellites in a stable orbit can be predicted to very high accuracy and are predictions for a particular location are available from the Heavens-Above website [18]. Due to the lower angular speed of the satellites, they may be detected down to peak magnitude of 0.

Satellite flares have an almost symmetrical trail if captured within a single frame, and as such this can be taken into consideration when trying to identify if a particular trail is unknown satellite or a meteor; whose trails may take on different forms.

Figure 26: A magnitude -7 Iridium satellite flare over the University of Hertfordshire's Learning Resource Centre in 2007, easily visible despite being in the flare of floodlights.

Date - Time	Magnitude	Satellite	Altitude
05/02/10 19:23	-5	Iridium 34	43°
05/03/10 19:35	-8	Iridium 76	52°
06/04/10 2:10	-6	Iridium 13	65°
08/04/10 2:06	-4	Iridium 18	62°
12/04/10 20:08	-1	Iridium 35	56°
12/04/10 21:34	-3	Iridium 25	56°
13/04/10 1:55	-5	Iridium 25	81°
14/04/10 21:33	-5	Iridium 13	29°
18/04/10 1:43	-1	Iridium 63	30°
20/04/10 1:41	-4	Iridium 72	35°
21/04/10 1:34	-1	Iridium 62	34°
24/04/10 1:25	-4	Iridium 38	70°
24/04/10 2:34	-1	Iridium 19	3°
24/04/10 2:47	-1	Iridium 22	22°

Table 4: A table of Iridium flares imaged by the camera and identified during 2010 [22].

Figure 27: A variety of flares matched to predictions for Iridium satellites, ranging from magnitude -4 to -8

Non-flaring satellites with a sufficiently high brightness and low angular speed can also be detected as constant trails across the sky.

The International Space Station (ISS) is easily visible, have a maximum magnitude as of its configuration in early 2010 of -3.5, and when transiting directly overhead may take over 6 minutes to cross the sky. In addition during times between launches and landings of the NASA space shuttle and docking/undocking with the ISS the shuttle itself is visible at a magnitude of around 0 [18]. During these times they are easily identified as they appear to follow each other across the sky along the same path,

Figure 28: A frame on the left from the morning of 18th April 2010, and on the right the morning of 19th April 2010. The International Space Station (right-most trail) can be seen trailing behind the Space Shuttle Discovery which had undocked on the 17th. The separation increased as Discovery prepares for re-entry.

An animation of the frames showing the 'chase' of the ISS and Space Shuttle Discovery across the sky was featured on the homepage of the popular website SpaceWeather.com on 19th April (http://spaceweather.com/submissions/large_image_popup.php?image_name=David-Campbell-iss-discovery_1271578125.gif)

Air Traffic

Due to its location near the busy airspace of London, Bayfordbury has a higher share of air traffic from commercial aircraft over its skies than many other observing sites. The number of aircraft trails visible between sunset and midnight, when the amount drops off, is typically between 90 and 120. This represents an average rate of around one every 3 or 4 minutes. Given this rate and the small angular size of an aircraft, the threat of disruption from trails during a telescopic exposure is minimal, however aircraft at high altitudes may leave contrails which expand over time and can persist for several hours.

The eruption of the Icelandic volcano Eyjafjallajökull in mid-April 2010 gave a unique opportunity to view the sky free from air traffic between 15th April and 20th April as European airspace was closed due to the adverse affects of volcanic ash [19]. This period also coincided with a (previously existing) period of clear weather. Although 17th April was the first night recorded since observations began in October to have no visible clouds throughout the entire night, it is not possible to know whether the lack of air traffic had any part to play, although there is at least one studying recognising the link between aircraft contrails and the formation and persistence of cirrus clouds [20] [21].

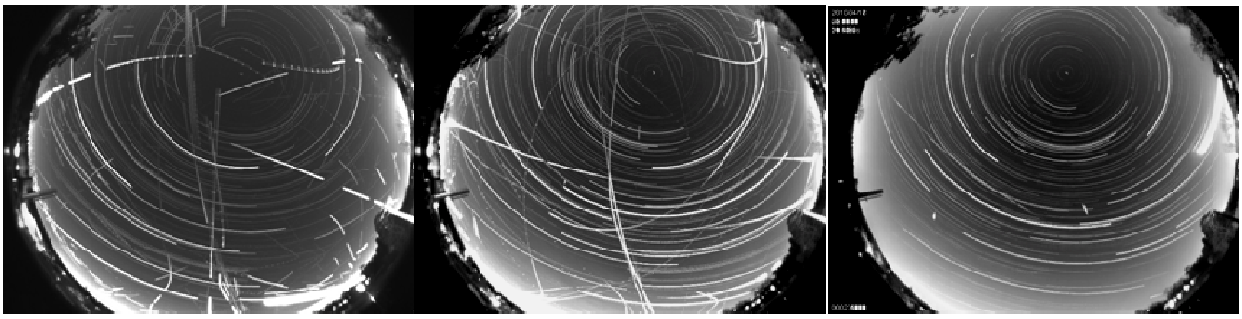

Figure 29: A stack of all of the frames from three clear nights. On the left and centre from March and December, with normal amounts of air traffic, on the right the night of 17th April, also the only night recorded with no visible clouds. The only trails present apart from celestial objects are from satellites, the International Space Station and Space Shuttle Discovery.

Conclusion

The computer will serve as a valuable tool for future students doing observations at Bayfordbury. The images allow a good quality view of the entire sky to be visible from any internet accessible computer, including those in the Patrick Moore Building and inside the domes. This would allow easy monitoring for potential clear sky from inside during cloudy conditions, as well as being able to monitor for incoming clouds from inside a dome, without having to step keep stepping outside. In addition, the excellent sensitivity of the camera allows faint clouds to be detection, which may not be visible to the naked eye without dark adaption after walking out of a lit building. In addition it would allow accurate records of the sky conditions when a practical was done to be known at a later date.

The analysis of weather conditions over the 6 month period have provided useful statistics for the characterisation of the site for comparing with others. 13.6% of all nights were found to be photometric – with 6 continuous hours of clear sky, and 35.7% of nights were spectroscopic – over an average of 2 per week. This was taken over winter and early spring months, and during a particularly poor winter, and would be expected to improve during summer. However, these values for comparison are between 20-30% the amount of photometric nights, and 45-60% the amount of spectroscopic nights that occur at the best astronomical observing sites throughout the world.

That each and every image from every night is archived in its raw form may prove to be an important asset in future, where observations of an object are unavailable before an event such as a supernova, outburst or unexpected star variation. Calculations show that fireball magnitude meteors that travel through the field of view of the camera should be detected, and that any meteors which are picked up are likely to be over this threshold, and of individual scientific note.

The feasibility of measuring the magnitude of variable stars was much less than initially anticipated, however given good enough conditions over the period of maximum brightness, Mira can be observed and accurate enough photometric measurements be taken to allow the approximate identification of the maximum point in its light curve.

References

[1]. **Santa Barbara Instrument Group.** Operating Manual AllSky-340 and AllSky-340C CCD Cameras. *SBIG Astronomical Instruments.* [Online] 30 June 2009. [Cited: 20 April 2010.] http://www.sbig.com/pdffiles/Allsky340%20Manual.pdf.

[2]. **Eastman Kodak Company.** Kodak KAI-0340 Image Sensor Datasheet. *Kodak.* [Online] 6 June 2009. [Cited: 20 April 2010.] http://www.kodak.com/global/plugins/acrobat/en/business/ISS/datasheet/interline/KAI-0340LongSpec.pdf.

[3]. **Fujinon Corporation.** Fujinon FE185C046HA-1 and FE185C057HA-1 Datasheet. *Fujinon CCTV Fish-Eye Lenses For Security.* [Online] [Cited: 20 April 2010.] http://www.fujinon.co.jp/en/products/cctv/pdf/a_1.pdf.

[4]. **Met Office.** Met Office: Coldest UK winter for over 30 years. *Met Office: Weather and climate change.* [Online] 1 March 2010. [Cited: 21 April 2010.] http://www.metoffice.gov.uk/corporate/pressoffice/2010/pr20100301.html.

[5]. **Meeus, Jean.** *Astronomical Algorithms 2nd edition.* Richmond : Willmann-Bell, Inc., 1998. ISBN 0-943396-61-1.

[6]. **Weisstein, Eric W.** Lambert Azimuthal Equal-Area Projection. *MathWorld--A Wolfram Web Resource.* [Online] 18 February 2004. [Cited: 20 April 2010.] http://mathworld.wolfram.com/LambertAzimuthalEqual-AreaProjection.html.

[7]. **Sarazin, Ed. M.** *VLT Site Selection Working Group final report, VLT Report 62.* 14 November 1990.

[8]. *Ten Years of Weather and Observing Statistics in San Pedro Martir, Baja California, Mexico.* **Tapia, M.** 179, Revista Mexicana de Astronomia y Astrofisica : s.n., 1992, Vol. 24.

[9]. **ESO.** 14. Site Characterisation. *ESO.* [Online] 05 July 2004. [Cited: 17 February 2010.] http://www.eso.org/sci/facilities/eelt/owl/Blue_Book/14_Site_characterization.pdf.

[10]. **Buil, Christian.** Iris Software. *Iris Software.* [Online] 5 February 2010. [Cited: 17 February 2010.] http://www.astrosurf.com/buil/us/iris/iris.htm.

[11]. **Met Office.** Met Office: Time and Place. *Met Office: Weather and climate change.* [Online] 19 November 2008. [Cited: 23 February 2010.] http://www.metoffice.gov.uk/newmedia/datafeed/time_and_place.html.

[12]. **Long, Kim.** *The moon book: fascinating facts about the magnificent, mysterious moon.* Boulder : Johnson Books, 1998. ISBN 1-55566-230-7.

[13]. **Richmond, Michael.** Atmospheric effects: extinction and seeing . *Michael Richmond's classes .* [Online] [Cited: 30 March 2010.] http://spiff.rit.edu/classes/phys445/lectures/atmos/atmos.html.

[14]. *Analysis of the fraction of clear sky at the La Palma and Mt Graham sites.* **della Valle, A., et al.** 3, Monthly Notices of the Royal Astronomical Society : Blackwell Publishing, 2010, Vol. 401.

[15]. **AAVSO.** Observations from the AAVSO International Database. *The American Association of Variable Star Observers.* [Online] [Cited: 2 April 2010.] http://www.aavso.org.

[16]. **International Meteor Organization.** International Meteor Organization . *Fireball observations.* [Online] [Cited: 21 April 2010.] http://www.imo.net/fireball.

[17]. *The visual appearance of the Iridium® satellites.* **Maley, Paul D. and Pizzicaroli, Joseph C.** 8, April 2003, Acta Astronautica, Vol. 52. ISSN 0094-5765.

[18]. **Peat, Chris.** *Heavens Above.* [Online] http://www.heavens-above.com.

[19]. **NATS.** NATS: The UK's leading Air Navigation Services Provider. [Online] [Cited: 21 April 2010.] http://www.nats.co.uk/index.html.

[20]. **British Broadcasting Corporation.** BBC News - How aircraft contrails form cloud. *BBC.* [Online] 8 January 2010. [Cited: 19 April 2010.] http://news.bbc.co.uk/1/hi/sci/tech/8309629.stm.

[21]. *A Case Study of the Radiative Forcing of Persistent Contrails Evolving into Cirrus.* **Forster, P., et al.** 2009, JOURNAL OF GEOPHYSICAL RESEARCH, Vol. 114.

[22]. **Richardson, James.** How Fast is "Swift": An Exploration of Meteor Angular Speeds. *Meteor Trails.* March 2000, No. 8.

[23]. **McBeath, Alastair.** Recent Fireball Sightings. *SPA Meteor Section.* [Online] http://www.popastro.com/sections/meteor/fireball_sightings.htm.

[24]. *Cloud Coverage Based on All-Sky Imaging and Its Impact on Surface Solar Irradiance.* **Pfister, G., et al.** 2003, Journal of Applied Meteorology, Vol. 42.

[25]. *Automatic cloud classification of whole sky images.* **Heinle, A., Macke, A. and Srivastav, A.** 2010, Atmospheric Measurement Techniques, Vol. 3.

[26]. **Pickering, T. E.** *The MMT All-Sky Camera.*

[27]. **Rutten, René.** CONCAM —ING's All-Sky Camera. *Isaac Newton Group of Telescopes.* [Online] 17 February 2004. [Cited: 11 March 2010.] http://www.ing.iac.es/PR/newsletter/news7/ins8.html.

[28]. **GIM Group.** Total Sky Imager (TSI). *Geophysical Instruments and Measurements Group.* [Online] [Cited: 11 March 2010.] http://www.gim.bnl.gov/instruments/tsi/index.html.

[29]. **Yankee Environmental Systems, Inc.** TSI-440 TOTAL SKY IMAGER. [Online] 11 September 2006. [Cited: 11 March 2010.] http://www.yesinc.com/products/data/tsi440/index.html.

Appendices

Appendix I: Hourly clear sky data

Data for the number of eighths of cloud cover for each hour of the night. Where no value is given, data was unavailable due to hardware issues, e.g. computer problems or condensation.

Date\Time	17-18	18-19	19-20	20-21	21-22	22-23	23-00	00-01	01-02	02-03	03-04	04-05	05-06	06-07	Average clear sky	Hours of clear sky
30 Oct 2009	8	8	8	8	8	8	8	8	8	8	6	5	8	8	4%	0
31 Oct 2009	3	4	4	6	7	6	7	8	8	8	8	8	8	8	17%	0
01 Nov 2009	4	5	7	7	6	4	4	7	2	3	3	0	0	0	54%	3
02 Nov 2009	8	5	6	7	7	7	7	8	8	8	8	8	8	8	8%	0
03 Nov 2009	1	3	0	0	5	7	7	7	6	6	0	0	0	0	63%	7
04 Nov 2009																
05 Nov 2009	8	7	6	7	8	8	8	8	8	8	8	8	8	8	4%	0
06 Nov 2009	8	8	8	8	7	0	4	4	4	4	1	1	3	2	45%	3
07 Nov 2009	5	2	0	0	4	5	7	8	8	8	7	8	8	8	30%	2
08 Nov 2009	7	7	7	7	7	7	7	7	7	7	7	7	8	8	11%	0
09 Nov 2009	7	8	8	8	8	8	8	8	8	8	8	8	8	8	1%	0
10 Nov 2009	8	8	8	8	8	8	8	8	8	8	8	8	8	8	0%	0
11 Nov 2009	8															
12 Nov 2009				8	8	7	8	8	5	1	8	8	8	8	13%	1
13 Nov 2009																
14 Nov 2009																
15 Nov 2009																
16 Nov 2009																
17 Nov 2009																
18 Nov 2009	8	7	7	8	8	8	8	8	8	7	7	7	8	8	4%	0
19 Nov 2009																
20 Nov 2009																
21 Nov 2009																
22 Nov 2009																
23 Nov 2009																
24 Nov 2009	8	8	8	8	8	8	7	8	8	8	8	8	8	4	4%	0
25 Nov 2009	2	6	4	0	0	0	1	3	7	2	2	1	1	0	74%	7
26 Nov 2009	4															
27 Nov 2009																
28 Nov 2009	8	8	8	8	8	8	8	8	8	8	8	4	3	6	10%	0
29 Nov 2009																
30 Nov 2009	7	3	6	1	0	1	2	1	6	0	0	0	0	0	76%	9
01 Dec 2009																
02 Dec 2009																
03 Dec 2009	8	8	8	8	8	7	2	1	5	7	7	7	5	0	28%	2
04 Dec 2009	8	8	8	8	8	8	8	8	8	8	8	6	6	0	11%	1
05 Dec 2009	8	8	8	8	8	8	8	8	8	8	8	8	8	8	0%	0
06 Dec 2009	1	0	0	0	0	0	4	7	8	7	6	7	7	8	51%	6
07 Dec 2009	8	7	8	8	5	7	6	8	8						10%	0
08 Dec 2009			8	8	8	8	8	8	8	6	8	5	5	8	8%	0
09 Dec 2009	8	8	8	8	8	8	8	8	7	8	0	0	0	0	29%	4
10 Dec 2009	2	1	1	1	2	3	4	4	4	4	4	8	8	8	52%	3
11 Dec 2009				8	8	8	8	8	8	4	1	8	8	8	13%	1
12 Dec 2009	0	1	0	1	1	3	2	6	8	7	7	7	8	8	47%	5
13 Dec 2009	7	8	8	8	4	7	3	3	3	2	3	8	8	8	29%	0
14 Dec 2009	8	8	8	8	8	8	8	8	8	8	8	8	8	8	0%	0
15 Dec 2009	7	0	7	8	8	8	8	7	7	6	6	6	7	8	17%	1
16 Dec 2009	8	8	8	8	8	8	8	8	7	5	1	2	4	3	23%	1
17 Dec 2009	0	1	7	8	8	8	8	8	8	8	8	8	8	5	17%	2
18 Dec 2009	7	7	8	8	8	7	2	0	1	7	1	5	6	4	37%	3
19 Dec 2009	4	3	5	7	8	8	8	8	8	8	8	8	5	3	19%	0
20 Dec 2009	0	0	0	0	0	0	0	0	2	4	3	0	0	0	92%	11
21 Dec 2009	8	8	8	8	8	8	8	8	8	8	8	8	8	8	0%	0

22 Dec 2009	7	8	8	8	8	8	8	7	4	7	7	8	7	8	8%	0
23 Dec 2009	8	8	8	7	8	8	7	8	8	8	5	7	8	8	5%	0
24 Dec 2009	8	8	8	8	8	8	8	8	8	8	8	8	8	8	0%	0
25 Dec 2009	0	0	1	1	0	1	1	4	3	2	5	7	7	7	65%	7
26 Dec 2009	7	4	3	3	3	4	4	0	0	0	0	1	1	3	71%	6
27 Dec 2009	5	1	0	0	0	2	8	8	8	7	7	8	7	7	39%	4
28 Dec 2009	8	8	8	8	8	8	8	8	7	7	8	8	7		3%	0
29 Dec 2009	8	8	8	8	8	8	8	8	8	8	8	8	8	8	0%	0
30 Dec 2009	8	8	8	8	8	8	8	8	8	8	8	8	8	8	0%	0
31 Dec 2009	7	8	7	7	3	5	5	7	7	6	3	1	0	0	41%	3
01 Jan 2010	0	0	0	0	4	5	8	8	8	8	8	8	8	8	35%	4
02 Jan 2010	7	7	8	8	8	8	8	8	8	8	8	8	0	0	16%	2
03 Jan 2010	0	0	0	0	0	0	0	1	5	8	6	0	0	0	82%	11
04 Jan 2010	0	1	4	4	5	1	1	2	4	5	6	8	8	8	49%	4
05 Jan 2010	8	8	8	8	8	8	8	8	8	8	8	8	8	8	0%	0
06 Jan 2010	8	7	7	4	4	1	1	0	0	2	1	3	2	3	62%	5
07 Jan 2010																
08 Jan 2010	0	3	8	5	7	0	0	0	7	1	2	0	0	6	65%	7
09 Jan 2010	8	8	8	8	8	8	8	8	8	8	8	8	8	8	0%	0
10 Jan 2010	8	8	8	8	8	8	8	8	8	8	8	8	8	8	0%	0
11 Jan 2010																
12 Jan 2010																
13 Jan 2010				8	8	8	8	8	8	8	8	8	8	8	0%	0
14 Jan 2010					8	8	8	8	8	8	8	8	8	8	0%	0
15 Jan 2010	8	8	8	8	8	8	8	8	8	8	8	8	8	8	0%	0
16 Jan 2010	8	8	8	8	8	8	8	8	8	1	0	0	0	0	35%	5
17 Jan 2010	0	0	0	0	0	0	0	2	4	8	8	8	8	8	59%	7
18 Jan 2010	8	8	8	8	8	8	8								0%	0
19 Jan 2010	8	8	8	7	7	8	8	8	8	8	8	8	8	8	2%	0
20 Jan 2010	8	8	8	8	8	8	8	8	8	8	8	8	8	8	0%	0
21 Jan 2010	5	7	8	8	8	8	8	8	8	8	8	8	8	8	4%	0
22 Jan 2010	8	8	8	8	8	8	8	8	8	8	8	8	8	8	0%	0
23 Jan 2010	8	8	8	7	8	8	8	5	6	7	8	8	8	8	6%	0
24 Jan 2010	8	8	8												0%	0
25 Jan 2010																
26 Jan 2010	1	2	3	5	2	2	1	4	8	8	8	8	8	8	39%	2
27 Jan 2010	8	8	8	8	3	6	8	8	8	5	7	8	8	8	10%	0
28 Jan 2010	8	8	8	8	8	8	8	8	8	8	8	8	8	8	0%	0
29 Jan 2010	1	2	1	0	0	0	0	0	0	0	6	7	7	5	74%	9
30 Jan 2010	1	0	0	0	0	0	0	0	0	0	1	0	1	2	96%	13
31 Jan 2010	7	1	0	0	0	0	0	3	8	8	5	0	0	0	71%	9
01 Feb 2010	1	5	1	3	2	2	5	6	8	8	8	8	8	8	35%	2
02 Feb 2010	4	6	7	8	8	8	8	8	8	8	8	8	8	8	6%	0
03 Feb 2010	8	8	8	8	8	8	8	8	7	8	8	8	8	8	1%	0
04 Feb 2010		7	6	4	8	7	8	8	8	8	8	8	8	8	8%	0
05 Feb 2010	0	0	0	0	3	3	3	2	5	7	6	6	6	3	61%	4
06 Feb 2010	8	8	8	8	8	8	8	8	8	4	8	8	8	8	4%	0
07 Feb 2010	8	8	8	8	8	8	8	8	8	8	8	8	8	8	0%	0
08 Feb 2010	8	8	8	8	8	8	8	8	8	8	8	2	1	1	18%	2
09 Feb 2010	5	4	6	4	5	6	8	8	8	8	8	7	7	4	21%	0
10 Feb 2010	4	3	0	1	7	8	8	8	8	8	8	8	8	8	22%	2
11 Feb 2010	0	3	6	7	8	8	8	8	8	8	8	8	8	8	14%	1
12 Feb 2010	8	8	8	8	8	8	8	8	7	5	7	8	8	7	5%	0
13 Feb 2010	7	7	6	8	8	8	8	8	7	8	6	8	8	8	6%	0
14 Feb 2010				8	8	8	8	2	7				8	8	11%	0
15 Feb 2010	8	8	8	8	8	8	8	8	8	8	8	8	8	8	0%	0
16 Feb 2010	8	8	8	8	8	8	8	8	8	8	8	8	8	8	0%	0
17 Feb 2010	0	0	1	3	4	5	3	4	4	6	8	8	7	7	46%	3
18 Feb 2010	8	8	8	8	8	8	8	8	8	8	8	8	8	8	0%	0
19 Feb 2010	1	2	2	0	0	3	0	1	0	0	0	0	1	5	87%	10
20 Feb 2010	4	2	3	4	0	0	0	0	0	3	7	8	8	8	58%	5
21 Feb 2010	7	8	8	8	8	8	8	8	8	8	8	8	8	8	1%	0
22 Feb 2010	8	8	8	8	8	8	5	0	2	8	7	8	8	8	16%	1
23 Feb 2010	8	8	8	8	8	8	8	8	8	8	8	8	8	8	0%	0
24 Feb 2010	8	8	8	8	8	8	8	8	8	8	8	8	8	8	0%	0

25 Feb 2010	8	8	8	8	8	8	8	8	8	8	8	8	8	8	0%	0
26 Feb 2010	0	0	0	0	0	4	3	2	6	8	8	8	8	8	51%	5
27 Feb 2010																
28 Feb 2010																
01 Mar 2010	2															
02 Mar 2010	1	2	2	2	3	4	4	5	6	7	7	7	8	8	41%	1
03 Mar 2010																
04 Mar 2010	0	0	0	0	0	0	0	0	0	3	8	8	8	8	69%	9
05 Mar 2010	2	3	3	6	8	4	0	3	8	5	6	8	8	8	36%	1
06 Mar 2010	0	0	0	0	0	1	2	2	3	0	0	0	0	0	93%	11
07 Mar 2010	0	0	0	0	0	0	0	0	0	0	0	0	0	0	100%	14
08 Mar 2010	8	8	8	8	4	6	6	3	2	6	6	8	8	0	28%	1
09 Mar 2010	8	8	8	8	8	8	8	8	6	2	8	7	8	8	8%	0
10 Mar 2010	8	8	8	8	8	8	8	8	8	8	6	1			9%	1
11 Mar 2010		8	8	6	1	2	8	8	8	8	8	8	8	8	14%	1
12 Mar 2010	8	8	7	8	8	8	8	8	7	8	8	7	8	8	3%	0
13 Mar 2010	8	8	8	8	8	8	8	8	8	8	7	7	5	1	11%	1
14 Mar 2010	0	0	0	0	7	1	0	0	0	3	4	6	8	1	73%	9
15 Mar 2010	7	7	6	6	0	2	0	3	8	8	8	8	8	8	29%	2
16 Mar 2010	1	2	3	3	4	5	6	6	8	7	4	3	7	8	40%	1
17 Mar 2010																
18 Mar 2010	8	8	8	8	8	8	8	8	5	6	2	1	8	5	19%	1
19 Mar 2010	8	8	8	8	8	8	8	8	8	8	8	8	8	8	0%	0
20 Mar 2010	8	8	8	8	8	8	8	8	8	8	8	8	8	4	4%	0
21 Mar 2010	2	0	0	0	0	0	1	3	4	8	8	8	8	8	55%	6
22 Mar 2010	8	8	7	1	0	0	0	0	0	2	6	8	8	8	50%	6
23 Mar 2010	8	8	8	8	8	8	8	8	8	8	8	8	8	8	0%	0
24 Mar 2010	5	8	8	8	8	8	8	8	8	8	8	8	8	8	3%	0
25 Mar 2010	8	7	8	5	0	7	4	6	8	7	6	1	3	2	36%	2
26 Mar 2010	8	8	7	8	8	8	8	7	8	8	8	8	8	8	2%	0
27 Mar 2010	8	8	5	6	0	0	0	0	4	3	6	7	8	8	44%	4
28 Mar 2010	8	8	8	8	8	8	8	8	8	8	8	8	8	8	0%	0
29 Mar 2010	8	8	8	8	8	8	8	6	7	8	8	8	8	8	3%	0
30 Mar 2010	8	8	7	2	3	1	3	6	7	8	7	8	8	8	25%	1
31 Mar 2010	8	6	5	0	1	4	4	6	6	7	7	4	3		41%	2
01 Apr 2010	8	2	6	7	8	8	8	8	8	8	8	8	8	8	8%	0
02 Apr 2010	6	1	1	6	7	2	5	5	7	7	8	8	8	8	29%	2
03 Apr 2010	8	8	8	6	7	8	8	8	8	8	8	8	8	8	3%	0
04 Apr 2010	1	1	1	0	1	3	6	7	7	8	8	8	8	8	40%	5
05 Apr 2010	5	2	2	6	8	7	8	8	7	3	1	2	4	4	40%	1
06 Apr 2010	8	8	8	8	8	8	8	8	8	8	8	8	8	8	0%	0
07 Apr 2010	8	8	8	8	7	7	6	2	0	0	0	0	0	0	52%	6
08 Apr 2010	2	1	1	3	3	1	1	0	1	2	2	2	3	2	79%	6
09 Apr 2010	8	8	7	6	7	7	7	5	4	1	1	2	3		37%	2
10 Apr 2010	7	7	7	8	8	7	7	8	8	8	8	8	8	8	4%	0
11 Apr 2010	4	1	3	8	8	8	8	3	7	8	8	8	8	8	20%	1
12 Apr 2010	0	0	0	0	0	0	0	1	1	8	8	8	7		68%	9
13 Apr 2010	3	8	8	8	8	6	8	8	8	8	8	8	8	8	6%	0
14 Apr 2010	1	0	2	0	0	0	3	6	8	8	8	8	8	8	46%	5
15 Apr 2010		1	3	7	8	8	8	6	4	8	8	8	8		20%	1
16 Apr 2010	1	1	0	0	4	8	8	8	8	8	8	8	8	8	30%	4
17 Apr 2010	0	0	0	0	0	0	0	0	0	0	0	0	0	0	100%	14
18 Apr 2010	8	8	7	8	8	7	8	7	2	4	7	8	8	8	13%	0
19 Apr 2010	8	8	8	8	7	2	2	1	2	6	5	0	0		45%	3
20 Apr 2010	0	0	2	8	7	4	0	0	0	0	0	0	0	0	81%	10
21 Apr 2010	4	4	3	4	4	6	8	8	7	7	7	7	6		28%	0
22 Apr 2010	4	4	4	3	4	5	6	7	8	7	7	7	7	3	32%	0
23 Apr 2010	5	5	5	6	6	7	7	6	6	6	6	6	6	7	25%	0
24 Apr 2010	6	6	6	7	7	7	8	8	8	8	8	8	8	8	8%	0
25 Apr 2010	8	7	1	0	0	0	0	0	0	6	0	2	1		76%	9
26 Apr 2010	4	2	1	0	0	1	2	0	0	0	0	0	0	2	89%	10
27 Apr 2010	6	3	4	5	6	6	6	6	7	8	8	8	8	8	21%	0

Appendix II: List of PHP program source codes

All algorithms for calculating the positions of celestial bodies are obtained from *Astronomical Algorithms 2nd edition* by J. Meeus [5].

a) AllSky live image overlay: **http://bus-winsrv2.herts.ac.uk/AllSky/overlay_code.htm**

   The overlay program also makes use of the following code:
   -A set of custom functions:
   http://bus-winsrv2.herts.ac.uk/AllSky/functions_code.htm

   -Periodic terms to calculate the positions of planets:
   http://bus-winsrv2.herts.ac.uk/AllSky/ptearth_code.htm
   http://bus-winsrv2.herts.ac.uk/AllSky/ptvenus_code.htm
   http://bus-winsrv2.herts.ac.uk/AllSky/ptmars_code.htm
   http://bus-winsrv2.herts.ac.uk/AllSky/ptjupiter_code.htm
   http://bus-winsrv2.herts.ac.uk/AllSky/ptsaturn_code.htm

b) File organiser: **http://bus-winsrv2.herts.ac.uk/AllSky/allskyorganiser_code.htm**

c) Automatic cloud detection: **http://bus-winsrv2.herts.ac.uk/AllSky/histogram_code.htm**